machines

Article

Design, Control and Stabilization of a Transformable Wheeled Fire Fighting Robot with a Fire-Extinguishing, Ball-Shooting Turret

Alper Kadir Tanyıldızı [ID]

Department of Mechatronics Engineering, Faculty of Engineering, Firat University, Elazig 23119, Turkey; atanyildizi@firat.edu.tr

Abstract: In this study, a hybrid wheeled fire extinguisher robot has been created. The robot has a two-degrees-of-freedom (DoF) fire extinguisher gun turret. To control the disruptive effect of mechanical oscillations on the firing system during movement of the robot body, PID and SMC controllers are used. When closed on flat ground, the robot's five-piece transformable wheel construction allows it to travel swiftly. The wheel mechanism opens on tough terrain, allowing the wheel to assume a star-shaped configuration and enabling the robot to ascend by grasping onto obstructions. The three-dimensional mechanical design of the firefighter robot was designed first, followed by the kinematic model of the turret system and the three-dimensional Simscape model in the Matlab Simmechanic environment. Simulations of throwing fire-extinguishing balls at fire locations positioned at 20 m to 80 m horizontal and 1–30 m vertical distances were carried out on this model for three different scenarios (the robot is stationary, moving at constant speed and rotating around itself). The simulations resulted in a shooting success rate of 85.71% with PID and 95.23% with SMC (for a total of 105 shots). When the mistake rates were investigated, it was discovered that the constructed fire robot was usable in firefighting.

Keywords: firefighting robot; transformable wheeled robot; fire extinguisher ball; shooting system; shooting stabilization

1. Introduction

The damage caused by fires to housing, industry, forest, facilities and equipment, infrastructure, and the environment reaches billions of dollars each year. In addition to material damage, loss of life, and extinction of plant and animal species also endanger human life. In our country, 2411 forest fires occurred in 2017, 2167 in 2018 and 2688 in 2019. The number of fires was 3350 in 2020, much more than the forest fires in previous years. In the last four years, a total of 10,616 and a yearly average of 2654 forest fires occurred. In these fires, 11,332 ha in 2019, 5644 ha in 2018, 11,993 ha in 2017 and 9156 ha in 2016 were damaged. Accordingly, the affected area in 2020 was well above the annual average of the last years (11,799). In 2020, 3350 forest fires occurred and a 20,870 ha area was damaged. The affected area per fire was 6.2 ha. In 2020, 10,545 fire workers, 4110 technical personnel and 6435 conservation officers were involved in the fight against forest fires [1,2]; 1072 water sprinklers, 281 water supply vehicles, 2267 first response vehicles, 185 dozers and 473 other vehicles are used in firefighting. In 2021, 2 aircraft and 27 helicopters were procured and used by firefighting services. Many volunteer and firefighter deaths and injuries occurred in the fires. There is a need for techniques that can fight fires more effectively and reduce the dangers to which firefighters are exposed [3].

Unlike monitoring forest activities, forest fire-extinguishing activities require direct intervention (traditionally through fire trucks and aircraft) in the forest environment to cause minimal damage not only to fauna and flora, but also to populations living in such places. Although forest monitoring via satellites is crucial in the fight against illegal

deforestation when forest fires occur, they do not contribute to fire extinguishment. In this case, this function is entirely dependent on the resupply of several crews of firefighters, water trucks and firefighters. In some cases, however, the environment of the fire site can be complex and variable, with varying degrees of toxic gas leakage and accumulation of unknown hazardous materials, significantly affecting the reconnaissance and safety of firefighters [4–7].

Early intervention and easy access to inaccessible environments during firefighting are extremely important in protecting living beings and firefighters from dangers. With the development of robot technology, the idea of fighting fires with unmanned robotic vehicles (land or air), which is the subject of this study, has emerged and has become popular among researchers [8,9]. Therefore, it is an important task to develop low-cost, powerful, economical and practical firefighting robots.

1.1. Related Works

Research about firefighting robots can be grouped under three main headings: structural design of firefighting robots [10–15], development of robot control systems [16–19] and development of environment recognition algorithms [20–22]. This study generally focuses on the first two titles, namely the structural design and control of firefighting robots.

Table 1 presents the seven basic characteristics (Locomotion System, Dimensions, Actuator type, robot size, Weight, Extinguisher Type, Maximum motion Speed, the fire response range of the robot) of the commercially produced firefighting robots in Figure 1. The environmental sensing, sensors mobility, motion control method, the ratio of the surface slope that the robot can move, and other features of these robots are examined and summarized in detail.

Robotic vehicles to be developed to fight fires can contribute to faster, safer and more efficient spraying of water or retarding agents in fire areas. The design of firefighting robots should be resistant to high temperatures and gas and dust concentrations, and in addition should have a high payload capacity and the ability to move effectively on rough terrain [8].

The FFR-1 (Figure 1p) firefighting robot is designed to work in narrow streets and indoors. Its mechanical structure is designed as a double-layer system, allowing it to operate in high-temperature environments. FFR-1 can work on stair steps. It can also climb 30-degree slopes with a 3-inch fire hose [9].

Guo et al. designed a small hybrid firefighting robot with wheeled legs in their study. The dimensions of the robot are $430 \times 420 \times 540$ mm and its weight is 30 kg [11]. Li et al. (2019) developed a fire reconnaissance robot to help firefighters by providing important information about a fire [12,13]. Alif et al. (2019) developed a firefighting robot called Qrob that can work in small and narrow spaces. QRob is designed more compactly than other conventional firefighting robots [14]. Ando et al. (2018) designed a robot that can fly directly to the fire source, fighting it with a water jet hose [15].

The first firefighting robots are Thermite RS1 and RS3. Thermite robots were developed by Howe Technology company in 2015. The Thermite firefighting robot is a remotely controlled robotic ground vehicle capable of high-definition, real-time video feedback. Its remote-control range is 300–500 m. The Thermite RS3 is a larger, faster version with higher water flow than Thermite RS1 [23,24]. RS1 24 hp and RS3 models work with 36 hp diesel engines. The RS1 has a maximum speed of 6 miles per hour, while the RS3 has a maximum speed of 8 miles per hour. The RS1 robot has a 1250 GPM nozzle (gallons per minute), while the RS3 has a 2500 GPM nozzle. The Thermite RS3 is equipped with a Positive Pressure Ventilation (PPV) ventilator system and its water spray rate is approximately 9464 L/min. These robots do not have a water tank. They are connected to an external water source with a hose [24].

Table 1. Summarized important features of firefighting robots.

Robot Name	Locomotion System	Dimensions (mm)	Actuator Type/Size	Robot total Weight (kg)	Extinguisher Type	Velocity (km/h)	The Fire Response Range of the Robot (m)
FFR-1 [9]	pallet	1620 × 1140 × 1380	electric motor	920	Water Flow	4	-
Thermite RS1 [23,24]	pallets	1962.15 × 1117.6 × 1625.6	24 hp diesel	725	Water Flow	6	-
Thermite RS3 [24]	pallets	3048 × 1666.24 × 1638.3	36 hp diesel	1588	Water Flow	8	-
TAF35 [25]	pallets	3000 × 1650 × 2200	71 hp diesel	3900	Water Flow	9	60–80
Colossus [26]	pallets	1600 × 780 × 760	24 V electric motor	485	Water Flow	3.5	-
Milrem Multiscope Rescue with Hydra and Hose Cartridge [27,28]	pallets	2400 × 2000 × 1150	hybrid diesel/electric motor	1630	Water Flow	20	-
MVF-5 [29]	pallet	3800 × 2180 × 2100	205 kW six-cylinder turbocharged diesel	16,000	Water Flow	12	-
Fire Ox [30]	6-wheel		10 hp diesel motor	-	Water Flow	-	-
LUF 60 [31]	pallet	2330 × 1350 × 2000	140 hp diesel motor	2200	Water Flow	6	60
FireMote-4800 [9,32]	pallet	1400 × 700 × 1140	electric motor	450	Water Flow	-	-
JMX-LT50 [9,33]	wheel	2440 × 1440 × 1560	diesel	1500	Water Flow	12	-
SACI 2.0 [9,34]	pallet	1800 × 1500 × 1600	electric motor	-	Water Flow	20	-
ArchiBot-M [9,35]	pallet	1400 × 800 × 650	-	450	Water Flow	20	-
MyBOT2000 [9,36]	pallet	1500 × 1000 × 1300	electric motor	910	Water Flow	2.36	-
Mitsubishi [3,37]	4-wheel	2170 × 1460 × 2070	-	1600	Water Flow	7.2	-
FireRob [9,38]	pallet	1300 × 685 × 385	-	240	Water Flow	3	-

The AirCore TAF35 crawler firefighting robot was developed in Italian EmiControls and German Magirus companies in cooperation in 2017. The AirCore TAF35 robot weighs 3.9 tons. It works with a 71-hp diesel engine. The robot can be controlled from 300 m away by remote control and its average speed reaches 9 km/h. Instead of spraying water with a hose, this robot transforms and spreads it into atomized water droplets forming a fog, thanks to the turbine on it. With a maximum water flow capacity of up to 4700 L/min, this robot is capable of effectively extinguishing large-scale forest fires. The fog technique is very effective for quickly removing heat from a fire. The fog emission range of the turbine extends up to 60 m [25].

A French company, Shark Robotics, developed the Colossus firefighting robot in 2017. Colossus is a remote-control robot with a range of 300 m. The robot has an electric motor and a 24 V battery. It can work non-stop for 5 h with its battery. Colossus is capable of moving at a maximum speed of 4.5 km/h over terrain with slopes of up to 40° and can climb obstacles of up to 30 cm. The chassis of the robot is made of lightweight and durable aluminum-welded aerospace steel with a total weight of 500 kg, capable of withstanding

thermal waves up to 900 °C. The Colossus has a water sprayer for firefighting. In addition, the robot has a day and night camera and a temperature detection sensor [26].

Figure 1. Firefighting robots (**a**) Termite RS1/RS3 [23,24] (**b**) TAF35 [25] (**c**) Colossus [26] (**d1**) Multiscope Rescue with Hydra [27] (**d2**) Multiscope Rescue Hose Cartridge [28] (**e**) Mitsubishi [3,37] (**f**) MVF-5 [29] (**g**) SmokeBot [3,39,40] (**h**) Lockheed Martin's Fire Ox [30] (**i**) LUF 60 [31] (**j**) JMX-LT50 [9,33] (**k**) FireRob [9,38] (**l**) Firemote-4800 [9,32] (**m**) SACI 2.0 [9,34] (**n**) ArchiBot-M [9,35] (**o**) Thermite T2 (**p**) FFR-1 [9,40] (**r**) MyBOT2000 [9,36].

Military Milrem Robotics Company carried out R&D studies together with Tartu and Tallinn Technology Universities and developed two different firefighting robot designs. The first of them has a water hose to extinguish the fire, and the other is a support robot designed to carry fire extinguishing equipment over long and difficult distances. The Milrem firefighting robot has a hybrid (diesel/electric) engine and lasts 10–12 h, moving at a maximum speed of 20 km/h. The robot's water/foam spray mechanism has a flow rate of 3000 L/min. The spraying range is 62 m. In addition, there are chemical sensors, visible light and thermal cameras on the robot [27,28].

The MVF-5 firefighting robot was developed by the Croatian company DOK-ING. The robot is powered by a six-cylinder turbocharged diesel engine with a power of 205 kW. There is a 2500 L water tank and a 500 L foam tank on the robot. The chassis of the robot is designed with material that can withstand 400 °C for 30 min and 700 °C for 15 min. The robot is remotely controlled up to a maximum distance of 1500 m. In addition, the robot has one thermal and eight high-resolution cameras and dangerous gas and radiation detection sensors. There is a rotating gripper mechanism in front of the robot. The robot can remove the obstacles in front of it via a gripper mechanism. It is stated that the maximum weight of the object it can lift is 10 tons [29].

Military product manufacturer Lockheed Martin Company produced a six-wheel drive (6WD) autonomous land vehicle for firefighting. The robot is driven by a 10 hp diesel engine. Fire Ox has a 12-gallon integrated foam cell and a 250-gallon polypropylene tank. This robot can also be controlled with a remote control and has RGB and Infrared (IR) cameras on it [30].

The LUF60 is a wheeled firefighting robot equipped with both air blast and water jet. The LUF60 robot is built from a material that can withstand 4000 degrees Fahrenheit. The robot can operate at a maximum surface inclination of 20 degrees. The robot has a nozzle with a flow rate of 800 GPM to spray the mixture of air and water into the fire. The spray range is up to 80 m [31].

The Firemote 4800 (Figure 1l) is a remote-controlled steel-insulated firefighting robot. It has a high-pressure water spray nozzle on it. The robot has navigation cameras and thermal imaging cameras to provide environmental sensing [32].

The JMX-LT50 is a remote-controlled firefighting robot. Thanks to its wheel structure, it can move on different terrain surfaces and overcome obstacles. There is a water tank on the JMX-LT50 firefighting robot, and it fights fire with a water jet. JMX-LT50 can spray pressurized water at different angles and distances [33].

The SACI firefighting robot is equipped with a trapezoidal pallet that allows it to overcome different obstacles. The robot is designed in such a way that it can spray water or foam on the fire or blow fog. The robot has a nozzle and a water tank that will produce 7600 L of water per minute. In addition, there are two foam tanks with a capacity of 25 L on the robot. The fire response range of the robot is a maximum of 60 m. The water spray nozzle of the robot can move vertically between 20 and 70 degrees. The SACI firefighting robot can work at full load capacity for six hours [34].

The Korean-designed ArchiBot-M firefighting robot has an independent suspension system specially designed for climbing stairs and working in high temperatures. The robot has a cooling system to operate at high temperatures [35]. The MyBOT2000 firefighting robot (Figure 1r), developed in Malaysia in 2006, has an electric motor. This robot is remotely controlled via a computer [36]. The nozzle of the robot can be controlled to extinguish fires at different heights. The MyBot2000 robot has an electric motor, along with state-of-the-art sensors and imaging systems.

Mitsubishi has developed a fire extinguishing platform within the scope of the project carried out jointly by the Japanese Mitsubishi Heavy company and the Japanese Fire and Disaster Management Agency (FDMA). The platform they developed is a special vehicle and carries two robots inside. The first robot is a four-wheeled fire engine equipped with a water tank. The second robot is a support robot that can extend hoses up to 300 m in length. Both robots have a laser range finder, a GPS, and an odometer. There is also an IMU sensor used to enable robots to navigate autonomously to a predetermined location. The firefighting robot can reach a maximum speed of 7.2 km/h and can spray water or foam up to 4000 L/min [3,37].

FIREROB is a tracked robot with sensors and a high-pressure water mist jet that can monitor the fire scene [9,38]. The SmokeBot robot, developed for responding to indoor fires, was developed in partnership with Sweden, England, Germany and Austria. The main task of the robot is to provide situational awareness in low visibility environments and to assist firefighters with its sensors. The robot has a radar camera that can create a 3D image

of its surroundings. The robot also has temperature chemical sensors to detect situations that may pose a threat to firefighters [3,39,40].

In addition to commercial firefighting robots, whose features are summarized in detail, there are also academic robotic design studies in the literature. For example, Zhang et al. designed a six-legged firefighting robot with three degrees of freedom in each leg. In addition, they produced the kinematic and dynamic model and carried out the movement of the robot legs with the parallel driving technique [10,41].

The fire extinguishing robots discussed above are very large fire extinguishers made for usage in open spaces with flat or low slopes. However, it has not been possible to locate a fire-extinguishing robot that is specifically designed to respond to fires inside industrial buildings. The majority of the vehicles described in the literature are relatively large, have limited maneuverability in small places, and are unable to pass over the stepped impediments that are likely to be present in large, multi-story facilities.

Within the scope of this study, a relatively compact firefighting robot with a hybrid transformable wheel construction that can operate both indoors and outdoors and is capable of ascending stairs has been presented. Unlike previous studies, this design replaces the water tank hose and fog turbine with a lighter and less space-consuming fire extinguishing ball and shooting turret. Although a conceptual design for the proposed robot has been presented, the primary goal of this study is to simulate the stabilization of the fire-extinguishing ball-firing system that will absorb the strong vibrations that will occur during movement when the robot finger mechanism is open and to demonstrate the effectiveness of the fire control.

1.2. Problem Statement, Contribution, and Novelty

Novelty and contribution of the designed hybrid fire-extinguishing robot with a transformable five-piece wheel structure.

➢ The robot's wheels will allow it to move fast over level ground.
➢ The wheel construction will transform into a finger structure and be able to ascend the step-like obstruction.
➢ There is a 2 DoF shooting turret on the robot. The turret throws a 1.3 kg fire extinguisher ball.
➢ A shooting stabilization controller was developed to improve the hit rate of fire extinguishing balls.
➢ The range of fire intervention has been increased to 85 m.
➢ A hybrid firefighting robot with a transformable wheeled shooting turret's kinematics and MATLAB/Simscape models were created.
➢ PID and SMC controller were designed for turret stabilization of the 2 DoF shooting turret.
➢ For three different motion scenarios (while the robot is standing and the robot is in motion, while the robot is turning to the right), fire extinguishing ball throws were executed at the fire zone at different heights and horizontal distances, and hit achievements were presented.

2. Materials and Methods

2.1. Transformable Wheeled Fire Fighting Robot with Fire Extinguishing Ball Controllersstem

In this study, the mobile firefighting robot has six transformable wheels and a throwing turret. The robot moves on a flat path in wheel mode. On rough terrain, the five-piece wheel mechanism opens and can climb obstacles. The 3D model of the firefighting robot was created using the SolidWorks™ 2020 program (Figure 2).
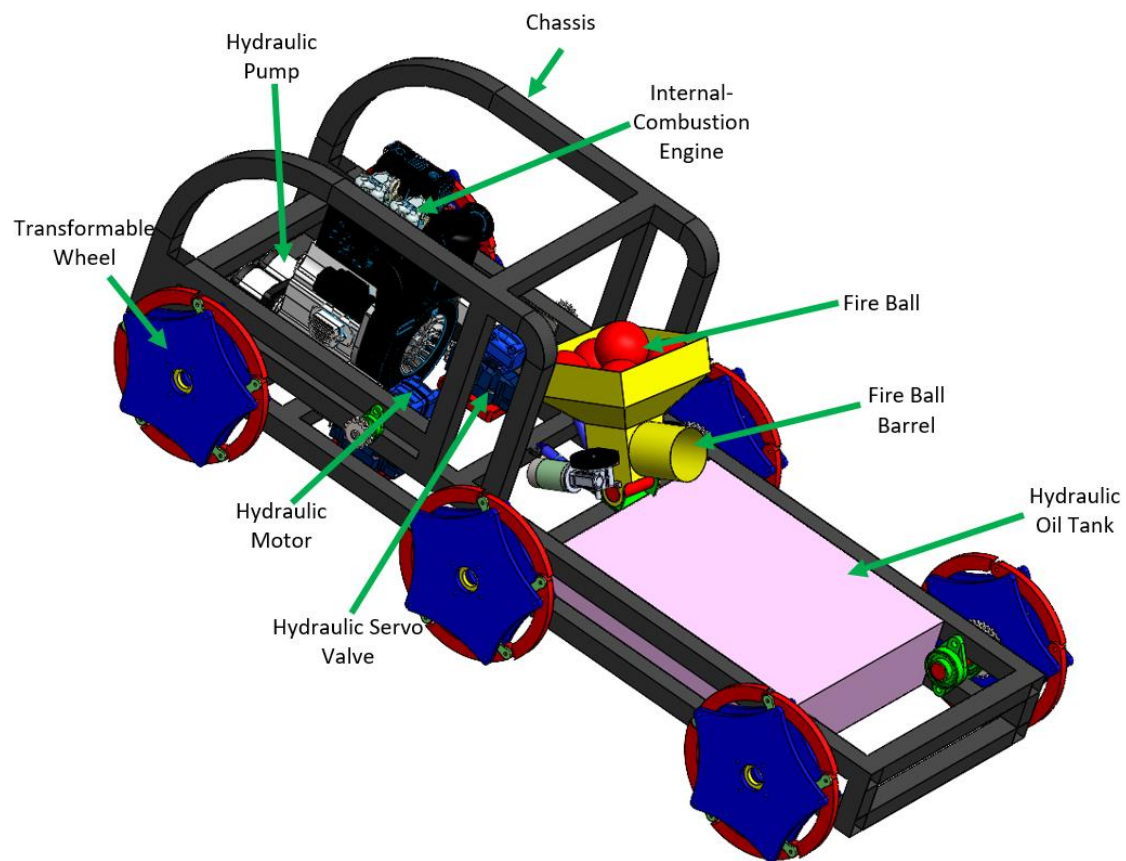
Figure 2. CAD views of designed Fire Fighting Robot with Fire Extinguishing Ball Shooting System.

Table 2 provides the parameter list for the fire-fighting robot's design with a mechanism for transforming wheels. The dimensions of the robot (width, length, height) are $1137.65 \times 2618 \times 954.5$ mm. It weighs 582.5 kg, making it lighter than any other robot designed for firefighting except Colossus [26] (500 kg). The robot has a total of six transformable wheels, three on the right and three on the left. The five-part transformable wheel opens up into the shape of a star. The wheel's diameter is 490 mm in closed mode and 900 mm in opened mode. The robot is driven by two hydraulic motors. One motor drives the right wheels and the other one drives the left wheels. Power transmission from the hydraulic motor to the wheels is provided by a chain-gear mechanism. The gear reduction ratio is 2. The firefighting cannon's turret uses a 2 DoF mechanism; it is located at the top and midpoint of the robot. A hydraulic pump is used to launch a fire extinguisher ball with a maximum weight of 1.3 kg to the point of the fire at a horizontal distance of 85 m and at a height of 30 m. The pressure of the hydraulic pump is 250–280 bar. The accuracy of the robot is assisted by stabilization.

The maximum speed of the robot is designed to be approximately 40 km/h when the wheel mechanism is closed. If we consider that hydraulic motors rotate with a maximum of 1000 rpm, since the gear reduction ratio is 2, the wheels can be driven with a maximum of 500 rpm. Since the diameter of the wheels with the partial wheel mechanism closed is 0.49 m, the distance traveled by the wheel in one revolution is approximately 1.54 m. When the wheel is rotated at max. 500 rpm, it will make 8.3 revolutions per second. Therefore, when multiplied by the amount of movement the wheel takes in one revolution, the vehicle's maximum forward speed will be $V = 1.54 \times 8.3 = 12.78$ m/s or approximately 46 km/h. Losses are considered negligible in these calculations.

Table 2. Robot specifications.

Part	Features	Values
Robot Dimensions	**Height**	954.5 mm
	Width	1137.65 mm (including wheel)–800 mm (except wheel)
	Length	2618 mm
	Weight	582.5 kg
Cannon (Turret)	**Length**	700 mm
	Location	Distance from front: 542.6 mm Distance from side: Right in the middle, 400 mm (excluding wheels)
Hydraulic Motor	**Transfer**	810 rpm (cont.)–1000 rpm (int.)
	Torque (int.)	240 N·m (cont.)–310 N·m
	Weight	12 kg
	Piece	Two. One drives the wheels on the left and the other those on the right.
	Power transmission mechanism	Power is transmitted by chain-gear on each side.
	Gear Reduction Ratio	2/The diameter of the gears connected to the wheels is twice that of the gear connected to the hydraulic motors.
	Piston	Two move the two axes of the shooting turret.
Hydraulic Pump	**Piece**	4 (2 for hydraulic motors and the other for oil transmission to the cylinders of the fire turret shooting turret.)
	Weight	114 kg
	Working Pressure (int.)	250 Bar (cont.)–280 Bar
	Flow	26.70 cc/dev
	Servo valve	4/The servo valve is used to precisely control the hydraulic oil flow. It is the unit that transfers the pressurized hydraulic oil from the pump to the engines in a controlled manner.
Diesel Engine (with reducer)	**Strength**	17 kW
	Max. Torque	50 N·m (2000 rpm)
	Weight	106 kg
Wheel Dimensions/speed/torque	**Closed**	490 mm
	Open	900 mm
	Rotation Speed	405 rpm (cont.)–500 rpm (int.)
	Torque	480 N·m (cont.)–620 N·m (int.)
Fire Extinguishing Ball Dimensions	**Weight**	1.3 kg
	Diameter	14.5 cm
Capacity	**Load Capacity**	10 fire extinguishing ball

When the vehicle is fully loaded, it is designed to be able to climb terrain with a slope of up to 45 degrees. Since the two hydraulic motors placed on both the right and left of the vehicle produce 310 N·m of torque each, they will produce a maximum of 620 N·m of torque in total. However, since the gear reduction ratio is 2, the total torque will be doubled, and it will be able to transmit 1240 N·m of torque to the wheels. The climbing slope was calculated considering that the vehicle climbs on sloping terrain when the fingers on the wheels are in the open position. With the wheels open, the wheel radius is 0.45 m and the traction force of the vehicle is found to be F = 1240/0.45 = 2755 N or 275.5 kg from the

torque/radius ratio. Since the total weight of the vehicle is 582.5 kg, the climbing slope is calculated as 0.472 or 47.2% from the ratio of 275.5/582.5. In these calculations, the losses are also negligible.

The vehicle is designed to be able to climb at its maximum speed on the ramp road with 20% slope, when the wheel fingers of the vehicle are closed. In this case, the slope angle of the road corresponds to 12° and the load force acting on the vehicle due to the slope of the road will be F = 582.5 × 0.2 = 116.5 kg or 1165 N. The power needed for the vehicle to climb this ramp is found as P = 1165 × 12.78 = 14.888 kW from the multiplication of the load force acting and the maximum speed. Considering the effects of aerodynamic load resistance and wheel-to-road friction resistance, which cannot be taken into account, it was thought that a 17 kW diesel engine would be sufficient for the vehicle.

The hydraulic pump and hydraulic motor selections were designed considering the torque and speed obtained from the crank output of the diesel engine. Hydraulic motors reach the maximum torque value when the wheels are open on sloping terrain; that is, in the case of maximum stress of the vehicle. The hydraulic motors can reach their maximum speed value on uneven, flat surfaces when the wheel fingers are closed, that is, in cases where the vehicle needs to accelerate to the maximum. Flow characteristics such as flow and pressure required by the hydraulic motor are covered by the hydraulic pump. The diesel engine continuously drives the hydraulic pumps at a constant speed of 2000 rpm. Wheel speeds can be controlled independently with the help of servo valves that direct each hydraulic motor separately. The right and left wheels can be driven at different speeds, and thus differential driving of the vehicle can be realized. The excess flow transmitted by the pump is sent to the hydraulic tank via the return line.

The hydraulic motors driving the wheels are fixed to the vehicle chassis. As can be seen in Figure 3, the rotational motion is transferred to the wheels by using a simple toothed chain system with a reduction ratio of 1/2.
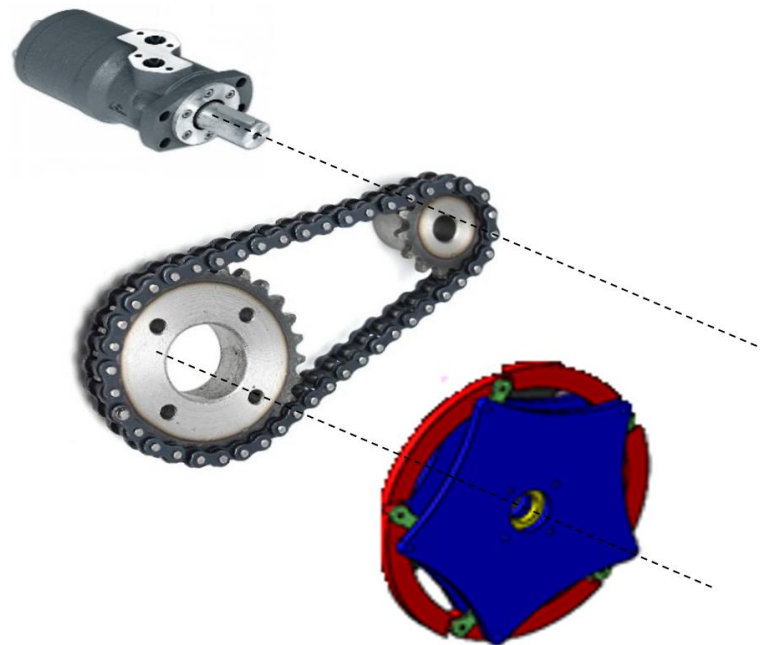

Figure 3. Wheel drive system of hydraulic motor with a gear-chain system.

In Figure 4, there are animation images reflecting the opening movement of the fingers with the transformable wheel mechanism. The middle disc is driven by a geared hydraulic motor. The gearbox used to increase the torque applied to the wheels has a ratio of 2. In addition, it is planned to have one motor for each of the 6 wheels to direct the finger movement.
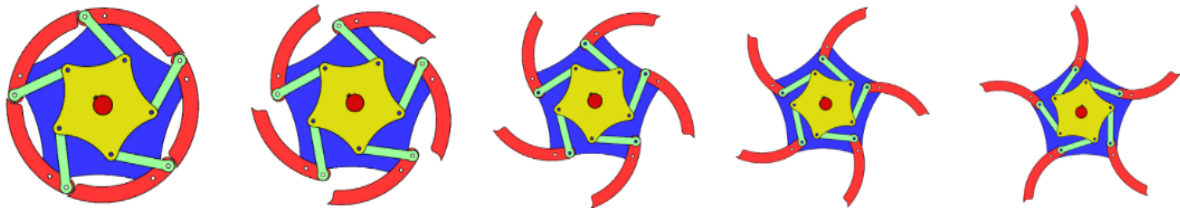
Figure 4. Animation of the mechanism that provides movement to the fingers.

The four-bar mechanism on each finger allows the wheel mechanism to be opened. Figure 5 shows the structure of a single finger's four-bar mechanism in order to make it easier to understand. L_1 represents the wheel disc in the open finger position, and L_1 is the fixed component of the four-bar mechanism. It is represented by the rotating middle disk member L_2, the connecting rod member L_3 and the finger member L_4. The four-bar mechanism's moving parts are L_2, L_3, and L_4. These notations $L\prime_1$, $L\prime_2$, $L\prime_3$ and $L\prime_4$ are stated with exponential quotation marks in the second position of the finger with the finger open.
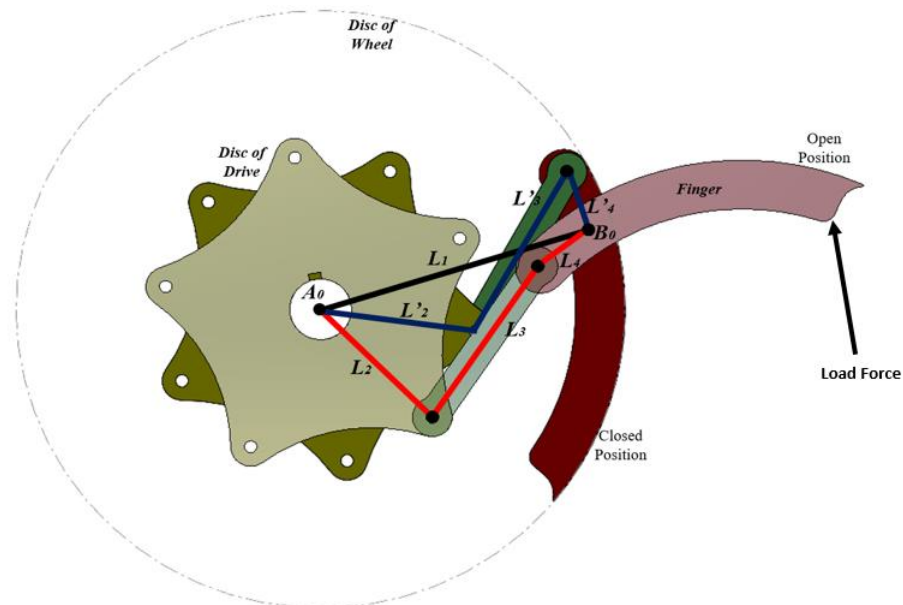

Figure 5. Four-bar mechanism for the movement of the fingers.

In order for the finger to be able to cover the load on it in the open position, the load torque corresponding to the B_0 joint should be calculated. Considering that the finger to be handled belongs to any wheel from the right or left wheel, it is assumed that it will encounter a load equal to half the weight of the vehicle. When the finger length is 0.2 m and the force acting on the tip of the finger is 2912.5 N, the product of these two values gives the Torque = $2912.5 \times 0.2 = 582.5$ N·m acting on the finger relative to the B_0 joint. The movement speed of the fingers is determined as max 1 r/s. Accordingly, the motor power to drive the finger mechanism was found to be P = 582.5 W by multiplying this load torque with the angular velocity.

As the firefighting robot moves with its fingers open across uneven ground, there will be vertical oscillations in its body. These oscillations in the robot's attempt to maneuver around the obstructions are crucial. However, while the robot is moving in wheel mode on level ground, oscillations and vibrations are not necessary for quick movement and navigating. Centrifugal forces can cause the fingers of a robot with a segmented wheel structure to spread out as it goes ahead in the closed position. To eliminate this disadvantage, the four-bar mechanisms are designed to be close to the dead position when the fingers are closed. The four-bar mechanisms are designed to be nearly in the dead position

when the fingers are closed in order to overcome this disadvantage. The dead position for the four-bar mechanism in Figure 6 is when the Ll_2 and Ll_3 elements are parallel to one another, and this is where the mechanism will go into lock mode. The mechanism can be retained in this position to decrease the energy used by the motor, allowing the fingers to remain closed. For a four-bar mechanism to fully open and close the fingers, the output rod (Ll_4) must make a pendulum movement at a total angle of $720°$.
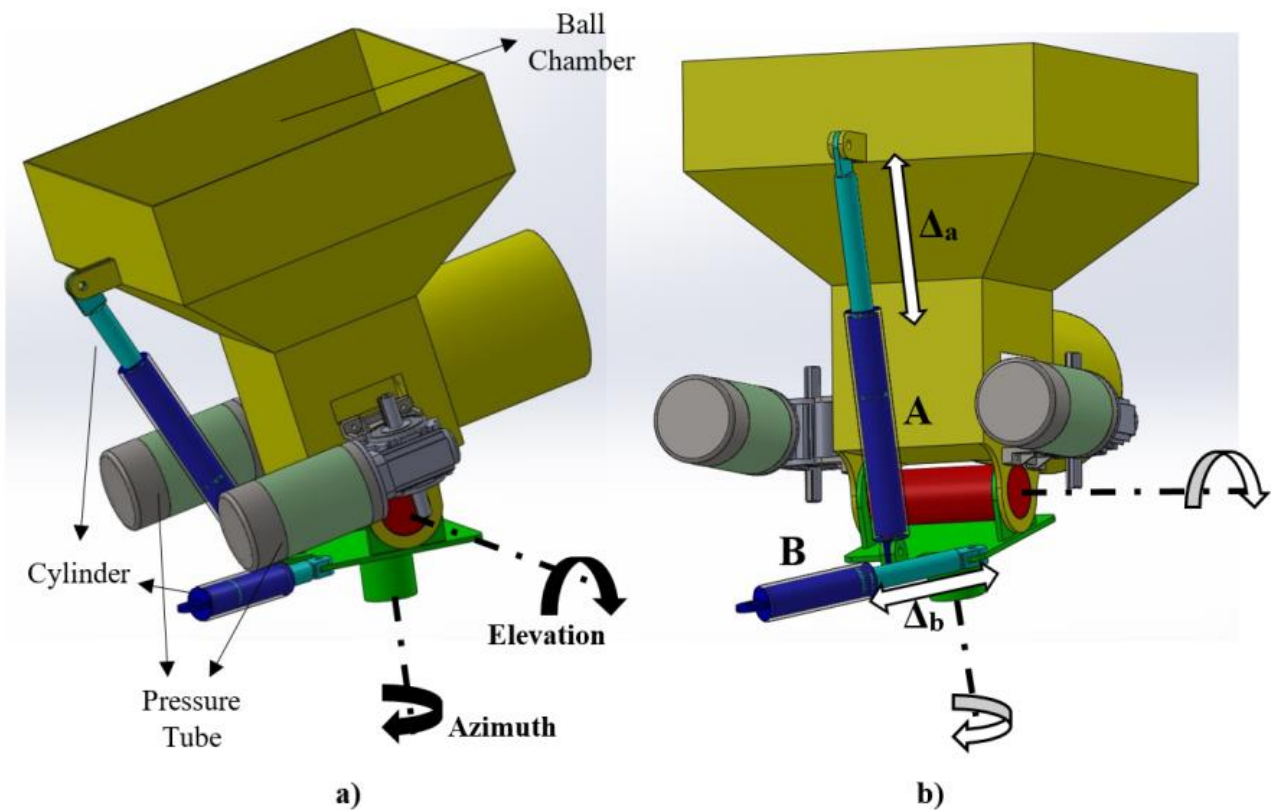

Figure 6. (**a**) Components used in the shooting turret (**b**) Shooting turret mechanism.

The elements used in the shooting turret mechanism are given in Figure 6a. Hydraulic cylinders were used for the circular movements of the shooting turret in the *azimuth* and *elevation* axes. The pressure required to launch the fire extinguisher balls into the turret chamber, however, is provided by pressure tubes. In Figure 6b, the details of the movement mechanism are given. The displacement Δa made by the cylinder A in the figure along the axis direction provides the circular movement of the tower in the *elevation* axis. In addition, the displacement Δb made by the B cylinder along the axis direction provides the circular motion of the tower in the *azimuth* axis.

2.2. Mathematical Modeling of Transformable Wheeled Fire Fighting Robot

The design and dimensions in the three-dimensional model are used to generate the robot's mathematical model. Assume that the robot's length is $2a$ and its width is $2d$. The finger length on the wheel is taken as L. The angular displacement of the rotate wheel is denoted by θ. The fingers are positioned at equally spaced angles with respect to the wheel center. In order to write the position expressions of the fingertips of each wheel, the axis set in the middle of the robot body was taken as reference and the Denavit–Hartenberg method was used. Figure 7 shows the arrangement of axes on the robot.
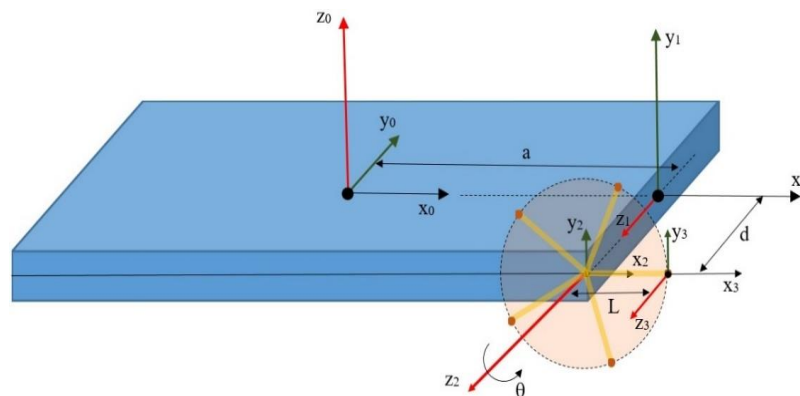
Figure 7. Robot kinematics image.

The link table necessary for the first finger was obtained by considering the wheel in the robot's front right corner, as shown in Table 3. The first finger is supposed to be positioned at zero degrees relative to the wheel center. The other fingers are placed at 72°, 144°, 216°, 288° positions, respectively, from the wheel center.

Table 3. First finger link table on right front wheel.

Link	θ	α	a	d
1	0	90	a	0
2	0	0	0	d
3	θ	0	L	0

According to the link table, A_1, A_2 and A_3 are transformation matrices. These matrices were calculated with the help of Equations (1)–(3). As a result of the multiplication of these matrices, the homogeneous transformation matrix T of the tip of the fingertip with respect to the robot body center was obtained with the help of Equation (4).

$$A_1 = \begin{bmatrix} 1 & 0 & 0 & a \\ 0 & 0 & -1 & 0 \\ 0 & 1 & 0 & 0 \\ 0 & 0 & 0 & 1 \end{bmatrix} \tag{1}$$

$$A_2 = \begin{bmatrix} 1 & 0 & 0 & 0 \\ 0 & 1 & 0 & 0 \\ 0 & 0 & 1 & d \\ 0 & 0 & 0 & 1 \end{bmatrix} \tag{2}$$

$$A_3 = \begin{bmatrix} \cos\theta & -\sin\theta & 0 & L\cos\theta \\ \sin\theta & \cos\theta & 0 & L\sin\theta \\ 0 & 0 & 1 & 0 \\ 0 & 0 & 0 & 1 \end{bmatrix} \tag{3}$$

$$T = A_1 A_2 A_3 = \begin{bmatrix} \cos\theta & -\sin\theta & 0 & a + L\cos\theta \\ 0 & 0 & -1 & -d \\ \sin\theta & \cos\theta & 0 & L\sin\theta \\ 0 & 0 & 0 & 1 \end{bmatrix} \tag{4}$$

The expressions obtained in Equations (1)–(4) are the general transformation expression of the tip point of each finger on the right front wheel with respect to the robot body center. Accordingly, the position expressions of the end points of each of the 5 fingers placed at equal angular intervals on the right front wheel relative to the robot body center can be calculated as follows. $\theta_1 = \theta$, $\theta_2 = \theta + 72°$, $\theta_3 = \theta + 144°$, $\theta_4 = \theta + 216°$, $\theta_5 = \theta + 216°$.

There are 6 wheels on the robot's body. Equations (5)–(9) were used to find the position of the finger tips on these wheels relative to the center of the robot's body.

$$p_{x1} = a + L\cos\theta_1, p_{y1} = -d, p_{z1} = L\sin\theta_1 \tag{5}$$

$$p_{x2} = a + L\cos\theta_2, p_{y2} = -d, p_{z2} = L\sin\theta_2 \tag{6}$$

$$p_{x3} = a + L\cos\theta_3, p_{y3} = -d, p_{z3} = L\sin\theta_3 \tag{7}$$

$$p_{x4} = a + L\cos\theta_4, p_{y4} = -d, p_{z4} = L\sin\theta_4 \tag{8}$$

$$p_{x5} = a + L\cos\theta_5, p_{y5} = -d, p_{z5} = L\sin\theta_5 \tag{9}$$

The positions of the five fingers of each of the six wheels are calculated with the same equations, but the parameters a and d are variable. The changes in the signs and values of the a and d parameters are summarized in Table 4.

Table 4. Parameter differences for wheels.

Wheel	Position	Parameters	
1	Right-Front	a	$+d$
2	Left-Front	a	$-d$
3	Right Middle	$a = 0$	$+d$
4	Left Middle	$a = 0$	$-d$
5	Right-Rear	$-a$	$+d$
6	Left-Rear	$-a$	$-d$

For the 3-axis independent rotation movements of the robot, Euler angles defined as in Figure 8 are used. The rotational motion of the robot around the x-axis is expressed as $R_x(\varnothing)$, the rotational motion around the y-axis is expressed as $R_y(\beta)$ and the rotational motion around the z-axis is expressed as $R_z(\gamma)$ (Equations (10)–(13)). Accordingly, the rotational transformation matrix R_{xyz} of any point on the robot can be obtained with Equation (14).

$$R_x(\varnothing) = \begin{bmatrix} 1 & 0 & 0 \\ 0 & \cos(\varnothing) & -\sin(\varnothing) \\ 0 & \sin(\varnothing) & \cos(\varnothing) \end{bmatrix} \tag{10}$$

$$R_y(\beta) = \begin{bmatrix} \cos(\beta) & 0 & \sin(\beta) \\ 0 & 1 & 0 \\ -\sin(\beta) & 0 & \cos(\beta) \end{bmatrix} \tag{11}$$

$$R_z(\gamma) = \begin{bmatrix} \cos(\gamma) & -\sin(\gamma) & 0 \\ \sin(\gamma) & \cos(\gamma) & 0 \\ 0 & 0 & 1 \end{bmatrix} \tag{12}$$

$$R_{xyz} = R_x(\varnothing) \times R_y(\beta) \times R_z(\gamma) \tag{13}$$

$$R_{xyz} = \begin{bmatrix} C\gamma C\beta & -S\gamma C\beta & S\beta \\ C\varnothing S\gamma + S\varnothing S\beta C\gamma & C\varnothing C\gamma - S\varnothing S\beta S\gamma & -C\beta S\varnothing \\ S\varnothing S\gamma - C\varnothing S\beta C\gamma & S\varnothing C\gamma + C\varnothing S\beta S\gamma & C\beta C\varnothing \end{bmatrix} \tag{14}$$
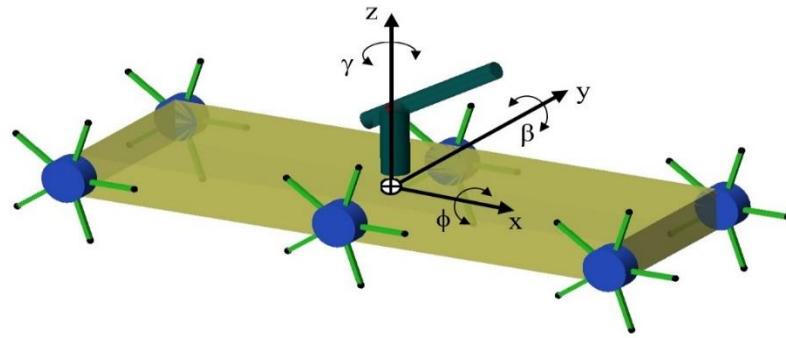
Figure 8. Euler angles of the robot body center.

2.3. Mathematical Modeling of Fire Extinguishing Ball Shooting Turret System

Fire extinguishing ball shooting turret system positioned on the robot has 2 DoF in Figure 9. It is in a pan-tilt position. The first axis enables the shooting control system to rotate $360°$ around the vertical axis. This vertical angle is represented as ϕ. The second axis enables the barrel to rotate around the horizontal axis with an angle of $180°$. This horizontal angle represented as ψ. Accordingly, p_G is the position expressions of the barrel tip relative to the robot center can be written as Equations (15)–(17) where d_t is the turret height and a_t is the barrel length.

$$p_{xG} = a_t \cos\psi \cos\varphi \tag{15}$$

$$p_{yG} = a_t \cos\psi \sin\varphi \tag{16}$$
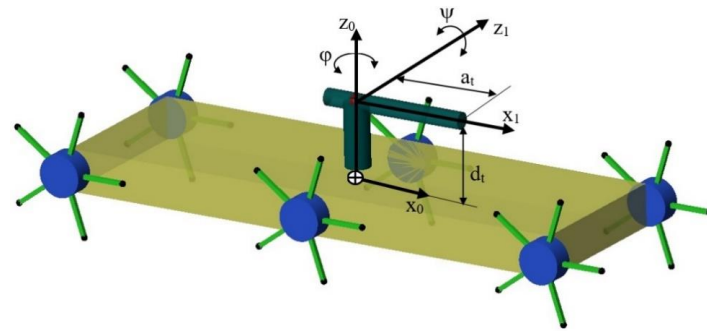
$$p_{zG} = d_t + a_t \sin\psi \tag{17}$$

Figure 9. Fire-Extinguishing Ball-Shooting Turret Control System.

The p_t position of the turret in the x, y, z axis relative to the robot center can be written as Equations (18)–(20).

$$p_{xt} = 0 \tag{18}$$

$$p_{yt} = 0 \tag{19}$$

$$p_{zt} = d_t \tag{20}$$

The P_{t0} position of the turret point relative to the ground on the shooting control system can be expressed as in Equation (21) depending on the T_{xyz} homogeneous transformation

matrix that defines the movement of the robot. Here, x_0, y_0, z_0 shows the translations of the robot on 3 axes.

$$p_{t0} = \begin{bmatrix} T_{xyz} \end{bmatrix} \begin{bmatrix} p_{xt} \\ p_{yt} \\ p_{zt} \\ 1 \end{bmatrix} \tag{21}$$

$$T_{xyz} = \begin{bmatrix} & & & x_0 \\ & R_{xyz} & & y_0 \\ & & & z_0 \\ 0 & 0 & 0 & 1 \end{bmatrix} \tag{22}$$

In the fire shooting control system, the necessary calculations for the barrel to be directed to the target were conducted by considering Figure 10. The position vector of the turret point relative to the ground on the moving robot is denoted by p_{t0}. The position vector of the fire point relative to the fixed location is shown with p_F. The vectorial difference p_E between these two vectors is determined as the linear vector that the barrel should orient on the turret and can be expressed by Equation (23).
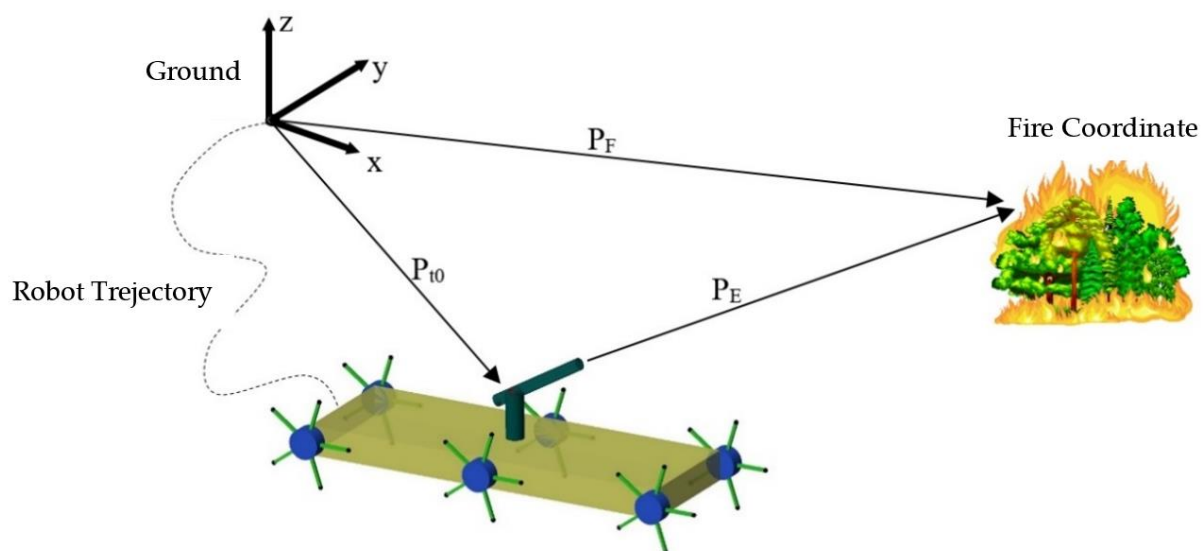
$$p_E = p_F - p_{t0} \tag{23}$$

Figure 10. Barrel orientation vector.

The resulting p_E error vector contains coordinates with respect to the fixed location. However, these coordinates need to be converted to moving coordinates on the robot. For this, the p_{Gt} vector is obtained with the help of Equation (24).

$$p_{Gt} = \begin{bmatrix} T_{xyz} \end{bmatrix}^T \begin{bmatrix} p_{xE} \\ p_{yE} \\ p_{zE} \\ 1 \end{bmatrix} \tag{24}$$

The p_{Gt} vector defines the position of the barrel relative to the turret and is obtained by multiplying the p_E error vector by the transpose of the homogeneous transformation matrix.

After determining the orientation vector of the barrel relative to the turret, p_{Gt}, elevation (φ) and azimuth (ψ) barrel orientation angles can be determined by using the inverse

kinematic expressions of the pan-tilt mechanism. In Equations (25)–(27), there are inverse kinematic expressions of the pan-tilt mechanism.

$$p_{Gt} = \begin{bmatrix} P_{xGt} \\ P_{yGt} \\ P_{zGt} \end{bmatrix} \tag{25}$$

$$\varphi = \tan^{-1}\left(\frac{P_{yGt}}{P_{xGt}}\right) \tag{26}$$

$$\psi = \tan^{-1}\left(\frac{P_{zGt}}{\sqrt{P_{xGt} + P_{yGt}}}\right) \tag{27}$$

However, as can be seen in Figure 11, since the fire-extinguishing ball leaving the barrel moves in an oblique manner, an additional correction angle must be added to the azimuth angle of the barrel in order to hit the target. For this, the function in Equation (28) is used depending on the distance and height of the target from the robot. The values of the constant coefficients in the function were determined by trial and error to increase the accuracy.

$$\psi_{ek} = \frac{4.55}{0.1^{\left(\frac{height}{200} + \frac{distance}{100}\right)}} \tag{28}$$
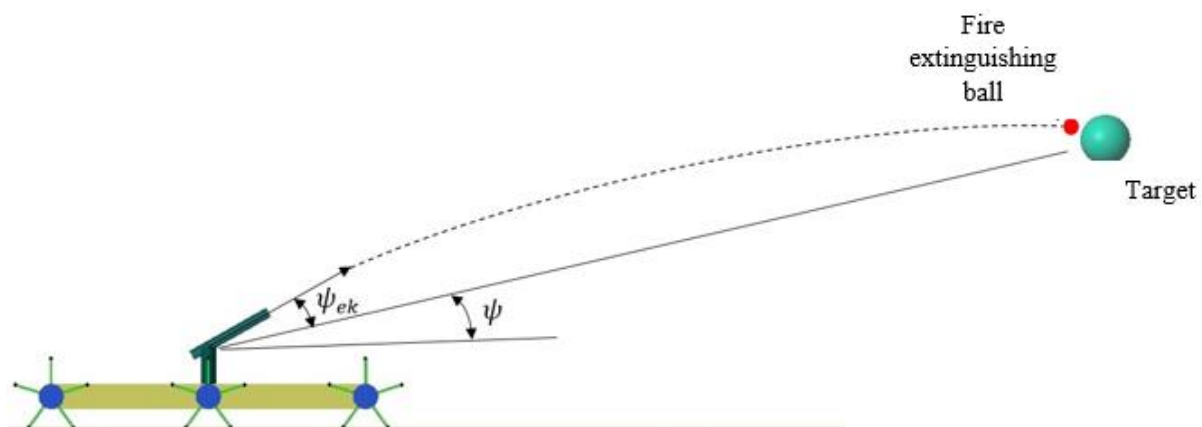

Figure 11. The oblique shot movement of the fire-extinguishing ball leaving the barrel.

Aerodynamic effects are included in the mathematical model of the fire-extinguishing ball from the moment it leaves the muzzle to its movement. Since the geometry of the fire-extinguishing ball is spherical, the air friction coefficient is taken as 0.3. The density of the air is assumed to be 1.25 kg/m^3. Since the velocity of the vehicle and the barrel that make up the system is low, apart from for the fire-extinguishing ball, aerodynamic effects are considered negligible. In addition, the effect of gravity is taken into account in the dynamic model created in the Simscape model in the Matlab Simmechanics environment. A detailed mathematical model of the turret's kinematic and dynamic model is included in our four-legged hunter robot article [42].

2.4. Control of Turret System

2.4.1. PID Controller Design

PID controller is designed to stabilize the azimuth and elevation angles of the fire control tower. For the optimization of the coefficients of the PID controller, the automatic optimization feature in the Simulink toolbox was used and the controller gain coefficients,

K_p, K_i and K_d, were determined. Equation (29) expresses how the PID controller generates the output signal versus the input signal [42].

$$u(t) = K_p e(t) + K_i \int_0^t e(t)dt + K_d \frac{de(t)}{dt} \qquad (29)$$

2.4.2. SMC Controller Design

The Sliding Mode Controller method is a control method that is resistant to parametric changes and external disturbances. As in this application, SMC gives successful results in the field of engineering for complex-structured and high-order nonlinear systems [42,43]. The 2 DoF firing turret is exposed to high-amplitude disturbance effects as it is located on the body of a transformable wheel robot. The basic working principle of SMC is to make the selected state variables converge to the selected slip surface [42,43]. Equation (30) expresses the slip surface.

$$s(t) = c e_1(t) + e_2(t) \qquad (30)$$

The sliding surface's slope is indicated by the true positive constant c. The tracing error values are $e_1(t)$ and $e_2(t)$.

$$e(t) = [e_1(t)e_2(t)] = [x_1(t) - dx_1(t)x_2(t) - dx_2(t)] \qquad (31)$$

d_t denotes the desired trajectory. For $s = 0$ condition, Equation (31), a linear homogeneous differential equation, is used. c represents the pole of the equation. According to the control law, the error asymptotically reaches zero when c is positive for any initial condition. According to the Lyapunov control law, for $V(s) = 0$ and $V(s) > 0$ for $s(0)$ can be defined as $V(s) = 1/2 \, s^2$. As a result, stability is guaranteed in the floating mode condition and a successful tracking performance can be achieved for $dV/dt = ss <= 0$. Equation (32) includes a control expression.

$$u(t) = K sign(s) \qquad (32)$$

In this study, the control output is the torque values that control the azimuth and elevation angles of the shooting tower. The most important disadvantage of the SMC control method is the chattering phenomenon. In order to eliminate this problem, the saturation function is used instead of the signum function in SMC control. Thanks to the system saturation function, it is aimed to keep the system response within a thin boundary layer of ε thickness with the slip surface instead of the slip surface itself. In this way, the chattering problem is eliminated [43] (Equation (33)).

$$sat(t) = \begin{Bmatrix} s > \varepsilon & 1 \\ s < -\varepsilon & -1 \\ -\varepsilon < s < \varepsilon & s/\varepsilon \end{Bmatrix} \qquad (33)$$

3. Simulation Setup and Results

The simulation model of the firefighting robot is shown schematically in Figure 12. The SimMechanics Multibody Model now includes a dynamic model that depicts the movement of the fire extinguisher ball used for shooting. Environmental factors, the speed at which the bullet exits the barrel, internal pressure during shooting, and the physical characteristics of the barrel are also taken into account in the dynamic movement of the barrel.

In this study, three separate shooting target scenarios were used to test the system's effectiveness. In the first scenario, the stationary fire-fighting robot launched the fire-fighting ball at the fire coordinates. In the second scenario, a fire-fighting ball was thrown to the fire coordinates while the robot moved steadily, and in the third case, the robot rotated about itself as the fire-fighting ball was delivered to the fire location.
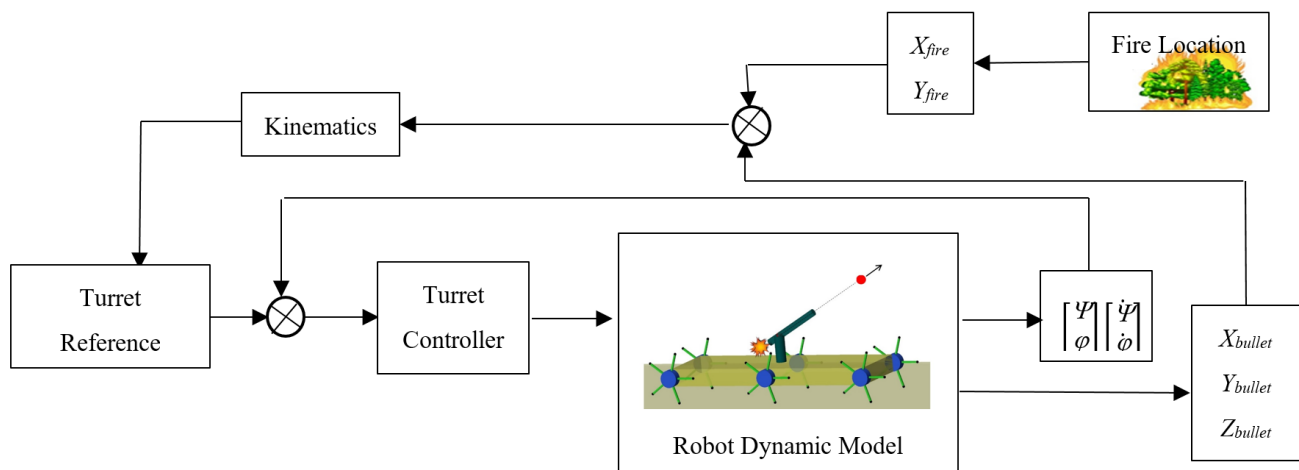
Figure 12. Schematic representation of firefighting robot SimMechanics Simscape multibody simulation model.

　　　The fire coordinates selected in the simulation are fixed points. The distance of the selected points to the robot varies between 20 m and 80 m horizontally and 1 m to 30 m vertically. About one second after the firefighter robot began to move, the shooting was carried out. The fire extinguisher robot and the fire area are thought to be 85 m apart at their closest point. The internal pressure of the barrel needs to be able to reach about 40 bar at the time of shooting in order for the fire extinguisher to reach this target, which is the furthest away. Figure 13 shows the change in the extinguishing ball's internal fire-extinguishing ballistic response over time. Accordingly, the output velocity of the fire extinguisher from the barrel was calculated as approximately 32 m/s.
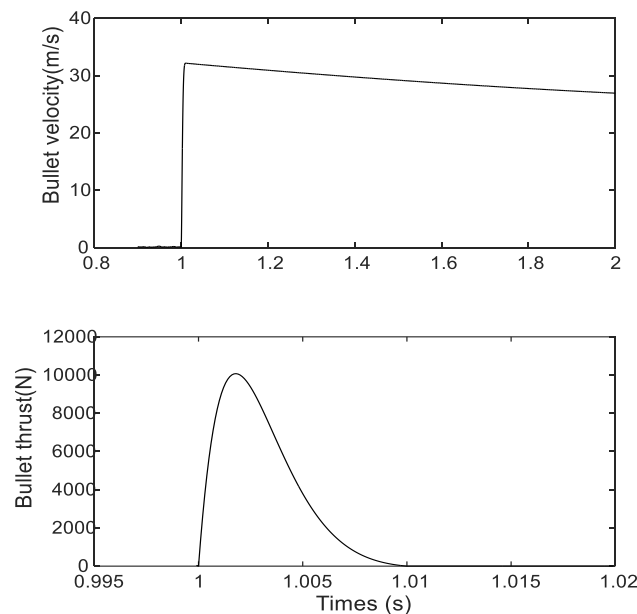
Figure 13. Internal fire-extinguishing ballistic response of the fire-extinguishing ball.

　　　PID and SMC controller and was designed for the position control of the shooting turret on the firefighting robot. The proportional, integral, derivative gain coefficients of the PID controller specified in Equation (29) and the slip slope c, *K* coefficients and ε value of the SMC controller specified in Equations (30)–(33) are presented in Table 5. In order to set the gain parameters of the controller at a good balance between performance and robustness, a crossover frequency (loop bandwidth) is determined based on the model dynamics and designed for a target phase margin of 60° in the first step. In the next steps,

optimum controller gain values are calculated for the algorithm by interactively changing the response time, bandwidth, transient response or phase margin using the controller tuner interface. All parameters were determined by using the closed-loop optimization method based on the frequency response of the turret Simscape model. The control output is limited to 500 N·m torque in accordance with the output torque of the hydraulic pump used in the design.

Table 5. Controller parameters of 2 DoF Turret.

Controller Type	Parameters
PID	K_p:100, K_d:10, K_i:1 for azimuth and elevation joint
SMC	$c_{azimuth} = 0.731$, $c_{elevation} = 0.729$, $\varepsilon = 0.001$ $K_{azimuth} = 29.98$, $K_{elevation} = 30.13$

3.1. Results of Scenario 1: Shooting Fire Extinguishing Ball While Robot Standing

In Scenario 1, the firefighter robot stops, which means that its speed is zero and that there is no body vibration that could disrupt the turret system. In these conditions, the PID and SMC controllers were used individually to perform the stabilization control simulation of the two degrees of freedom turret system. Fire extinguisher balls were thrown at the fire locations in the simulations that were spaced out over a range of seven different heights and horizontal distances, and hit successes were recorded. The hit errors caused by the gunfire when the fire extinguisher reaches the target coordinate are estimated in meters and shown in Table 6. If the fire extinguishing ball is within 5 m of the target, the shot is declared successful. The accuracy of the shots is highlighted in Table 6. As can be seen in Table 6, in the system where the PID controller is located, all the shots, except for one shot, remained within a 5 m circle. The shots outside the 5 m circle are written in bold in the tables. In the SMC-controlled system, the hit success is much higher, and all the fire extinguishing balls are delivered to the target within a 1 m circle.

Table 6. Accuracy errors of shots fired at targets from a stationary firefighting robot with PID and SMC.

Target Distance (m)	Target Height (m)									
	1		5		10		20		30	
	PID	SMC	PID	SMC	PID	SMC	PID	SMC	PID	SMC
20	0.73	0.9454	0.85	0.7906	1.01	0.6036	1.43	0.2682	2.07	0.0126
30	0.59	0.9265	0.80	0.8004	1.03	0.6452	1.41	0.3520	1.70	0.0893
40	0.30	0.9029	0.60	0.7941	0.93	0.6591	1.40	0.3979	1.40	0.1545
50	0.10	0.8748	0.50	0.7775	0.92	0.6564	1.42	0.4189	0.87	0.1922
60	0.19	0.8417	0.66	0.7526	1.13	0.6414	1.36	0.4216	0.64	0.2083
70	0.68	0.8028	1.12	0.7197	1.41	0.6158	0.45	0.4090	4.92	0.2061
80	1.25	0.7573	1.32	0.6785	0.81	0.5798	3.53	0.3826	**15.07**	0.1872

In accordance with scenario 1, a total of 35 shots were fired at the fire coordinates at different distances with the SMC and PID controlled turret system. Since it is not possible to display the elevation and azimuth control signal, trajectory, velocity and error graph of the turret system for each firing simulation, graphs are presented for a single firing simulation for both controllers. In the simulation for which the graph is given, the coordinates of the fire point are located at a distance of 60 m and at a height of 30 m from the robot. The control signals applied to the motors controlling the azimuth and elevation axes of the turret system, the reference and follow trajectory responses of the controller, and the position tracking error graphs are shown in Figure 14. The position response and error

graphs show that both controllers perform well at the tracking azimuth angle, but the SMC controller outperforms the PID controller when it comes to controlling the elevation angle.
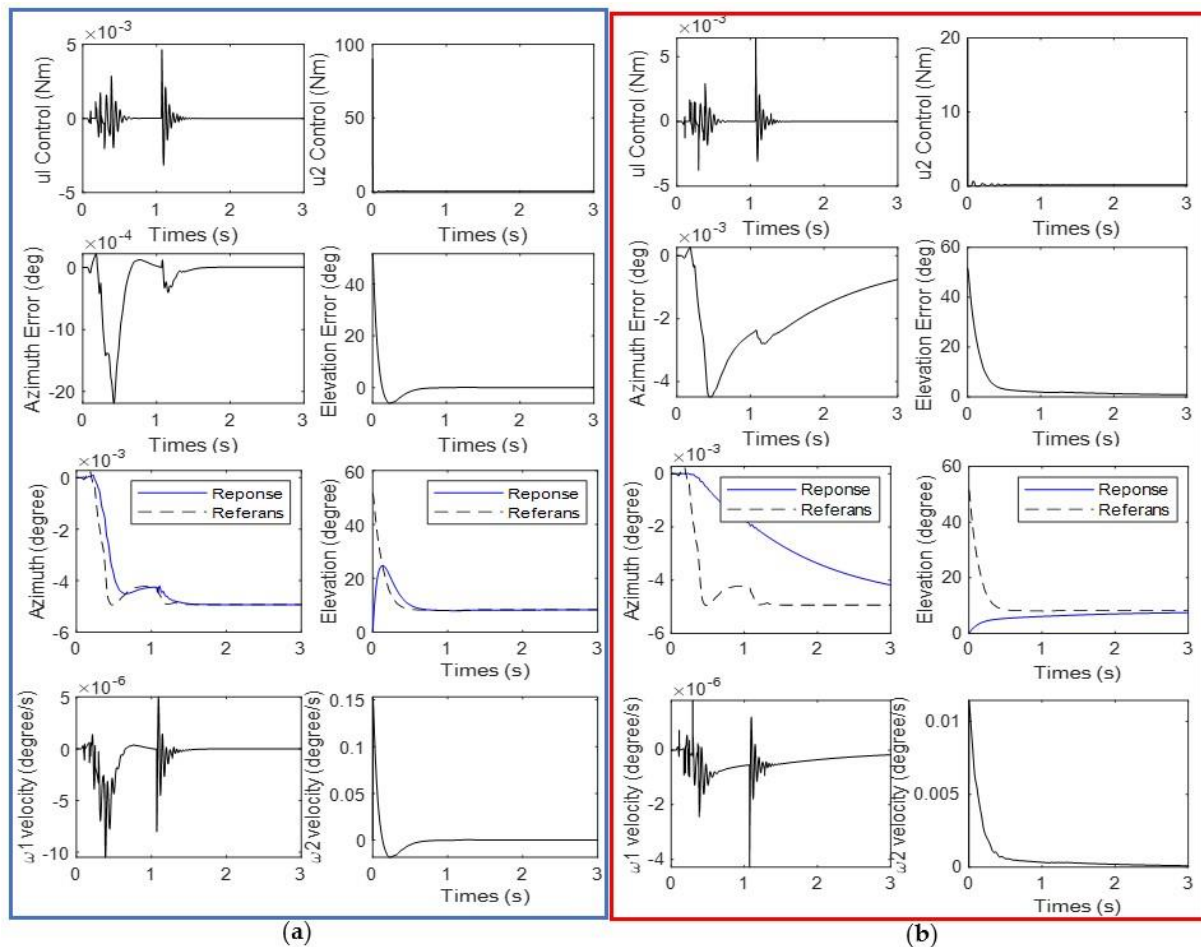

Figure 14. Control signals, error values, trajectory and velocity of Turret System elevation and azimuth motor with (**a**) SMC (**b**) PID controllers for Scenario 1.

3.2. Results of Scenario 2: Shooting Fire While Going Straight

In scenario 2, the robot has the wheel mechanism open and advances at a consistent speed on its fingers. Large oscillations take place in the robot body because the robot is moved with the fingers of the transformable wheels in the open position. Figure 15 shows how the firefighting robot's speed and position change over time. The progress rate of the firefighting robot in the x direction in 3 s is 1.5 m and its speed is approximately 0.5 m/s (7.2 km/h). The vibration amount φ around the x-axis in the 0–1 range during the first take-off is relatively high [0.005–0.005°] due to the first take-off inertia. After 1 s, the vibration of the robot in the x direction is very low. The β position change of the robot around the y-axis continues in the form of vibration at a certain frequency. The reason for these vibrations is the contact of the fingers placed at 72° angles with the ground. The swing angle γ around the z-axis is almost zero after the first take-off, that is, the 0–1 s interval. The displacement amounts, angular velocity change and vector velocity change graphs of the robot in the x, y, z axes are also seen in Figure 15. Approximately zero displacement occurs on the y and z axes on average, because the robot keeps moving forward in a straight line.
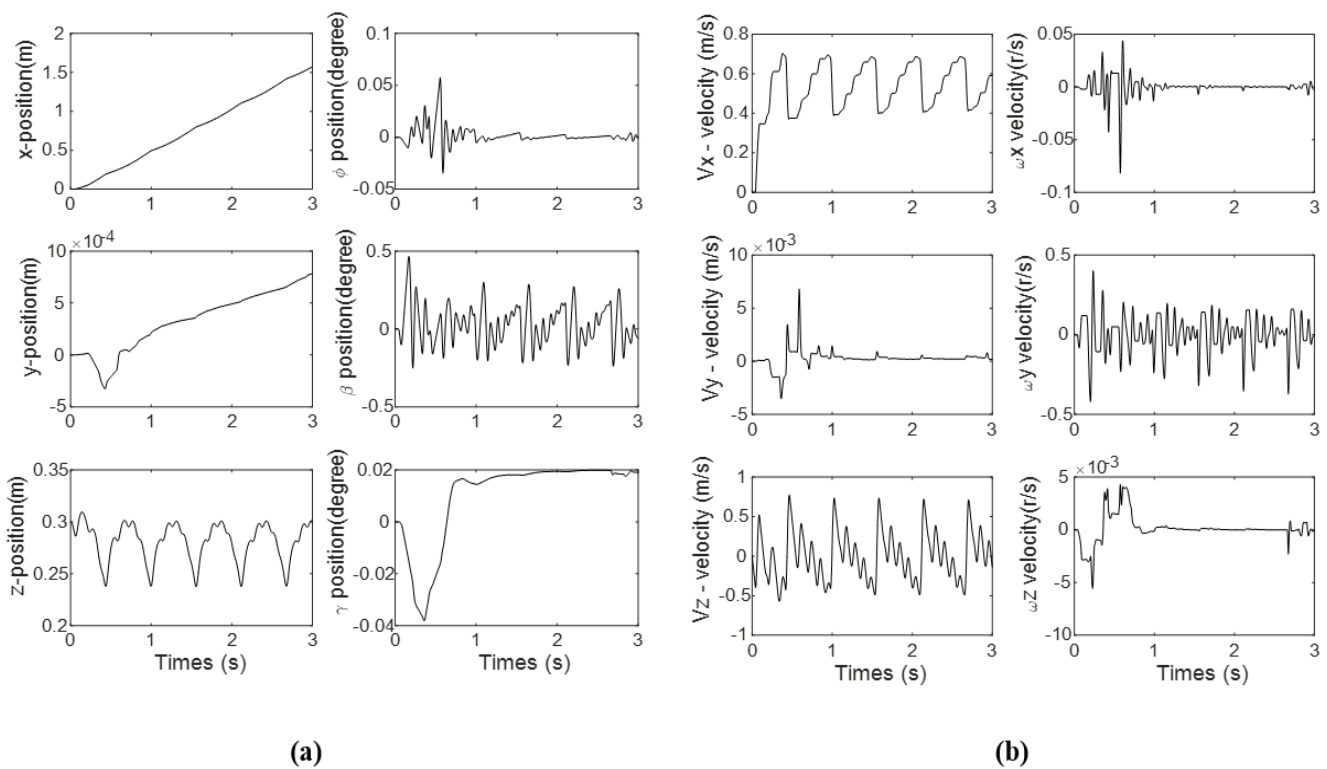
(a)

(b)

Figure 15. (**a**) The displacement response of the forward motion of the robot (**b**) The velocity response of the forward motion of the robot.

A fire-suppressing gun was discharged at the identical fire coordinates mentioned in scenario 1 while the Firefighter robot was moving at a steady speed and under the influence of hull vibrations operating on the turret. The simulation time is set to 3 s. Table 7 displays the scenario 2 outcomes of the fire extinguisher cannon shot simulation. If the fire extinguishing ball is within a radius of 5 m of the target, the shot is declared successful. Shots outside this area are shown in bold in the table. The shots outside the 5 m circle are written in bold in the tables. As can be seen in Table 7, in the system where the PID controller is located, all the shots except for three ended within a 5 m circle. In the SMC-controlled system, the hit success is much higher, and all the fire-extinguishing balls are delivered to the target within a 0.75 m circle.

Table 7. Accuracy errors of shots fired at targets from a moving straight forward robot with PID and SMC.

Target Distance (m)	Target Height (m)									
	1		**5**		**10**		**20**		**30**	
	PID	**SMC**	**PID**	**SMC**	**PID**	**SMC**	**PID**	**SMC**	**PID**	**SMC**
20	0.50	0.7217	0.68	0.5727	10	0.3929	1.39	0.0777	2.05	0.2067
30	0.18	0.7034	0.44	0.5820	0.90	0.4327	1.16	0.1532	1.43	0.1118
40	0.28	0.6807	0.04	0.5759	0.72	0.4460	0.91	0.1963	0.81	0.0570
50	0.68	0.6536	0.27	0.5599	0.41	0.4434	0.65	0.2162	0.10	0.0388
60	0.81	0.6217	0.32	0.5359	0.17	0.4290	0.26	0.2187	2.04	0.0395
70	0.54	0.5843	0.13	0.5043	0.12	0.4044	1.01	0.2086	**6.70**	0.0391
80	0.24	0.5405	0.22	0.4647	0.11	0.3699	**5.32**	0.1818	**17.08**	0.0398

In the simulation of scenario 2, the control signal and position-tracking error graphics applied to the motors in the azimuth and elevation axes of the turret system while the fire extinguisher is thrown to this point, with the fire target located at 60 m away and 30 m high from the robot, are presented in Figure 16.
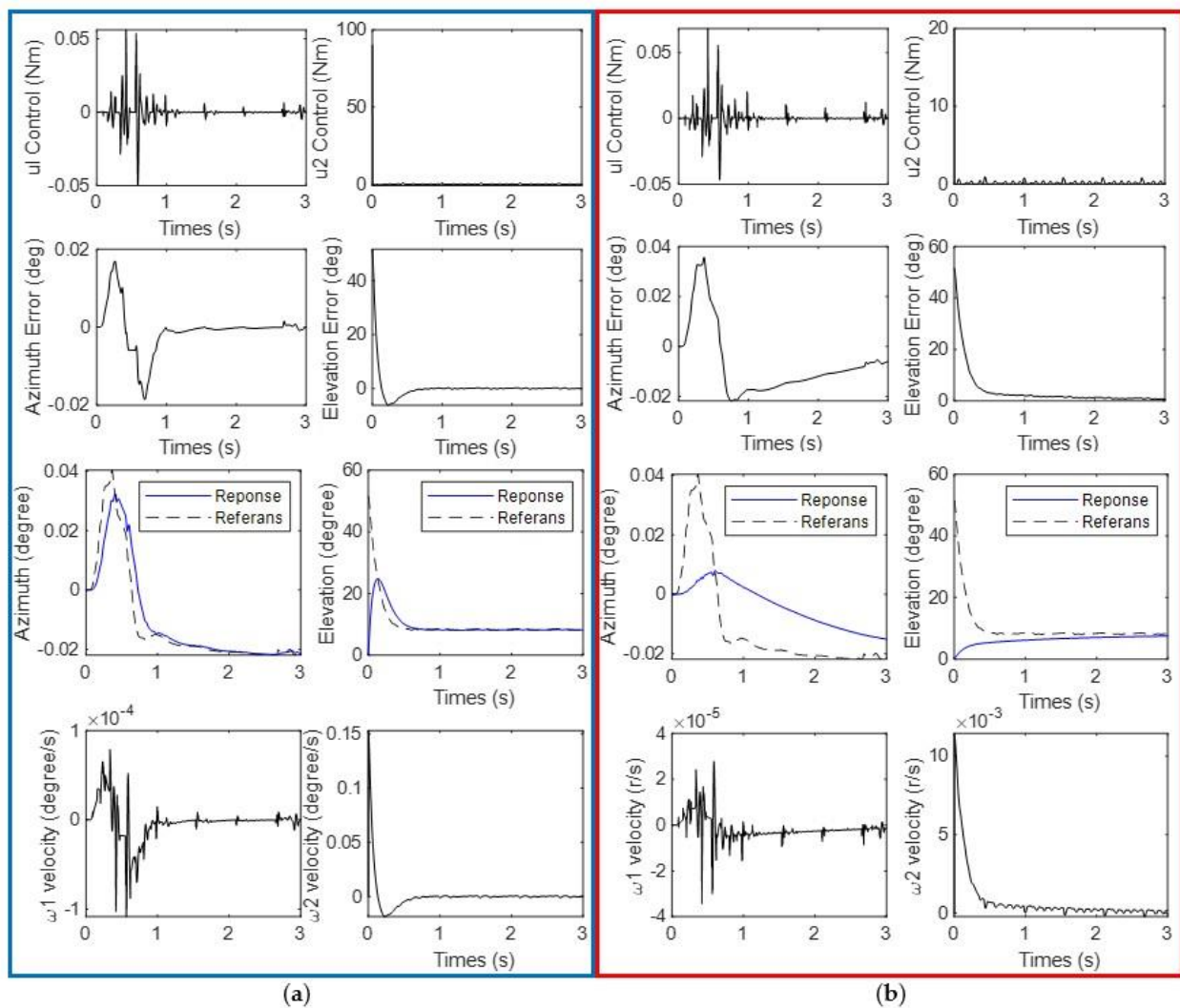
Figure 16. Control signals, error values, trajectory and velocity of Turret System elevation and azimuth motor with (**a**) SMC (**b**) PID controllers for Scenario 2.

3.3. Results of Scenario 3: Shooting Fire While

When the wheel mechanism is open in Scenario 3, the robot rotates from right to left at a steady speed on its fingers to respond to a fire in a restricted region. The robot fires a ball toward the coordinates at the same horizontal and vertical distances specified in the other two scenarios. The speed and position change of the robot body during the rotation movement are presented in Figure 17.

The scenario 3 results of the fire-extinguishing ball shot simulation are presented. As can be seen in Table 8, in the system where the PID controller is located, all the shots except for three remained within a 5 m circle. The shots outside the 5 m circle are written in bold in the tables. In the SMC-controlled system, the hit success is much higher, and all the balls are delivered to the target within a 1.8 m circle.
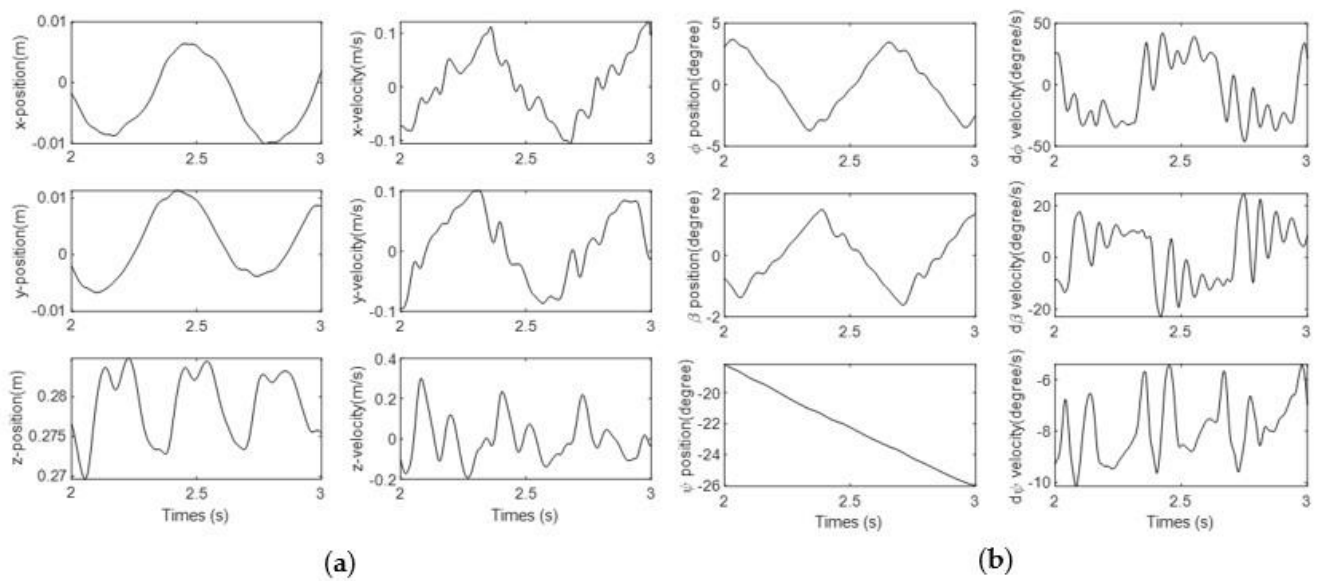
Figure 17. (**a**) Displacement response of the robot's 90° rotation (**b**) The velocity response of the robot's 90° rotation.

Table 8. Accuracy errors of shots fired from the firefighting robot at targets while making a right turn maneuver with PID and SMC.

Target Distance (m)	Target Height (m)									
	1		5		10		20		30	
	PID	SMC	PID	SMC	PID	SMC	PID	SMC	PID	SMC
20	0.43	1.7386	0.63	1.6558	10	1.5700	1.59	1.4619	2.52	1.4244
30	0.10	1.7287	0.40	1.6613	0.91	1.5880	1.46	1.4830	2.19	1.4323
40	0.42	1.7163	0.32	1.6588	0.76	1.5947	1.40	1.4969	2.10	1.4415
50	0.86	1.7018	0.61	1.6513	0.63	1.5944	1.49	1.5043	2.33	1.4487
60	1.05	1.6058	0.82	1.6400	0.73	1.5888	1.79	1.5062	3.47	1.4529
70	1.01	1.6660	1.05	1.6253	0.99	1.5790	2.60	1.5036	**7.38**	1.4540
80	1.28	1.6645	1.62	1.6075	1.41	1.5655	**6.14**	1.4972	**17.18**	1.4525

Figure 18 shows the control signal and position tracking error graphics applied to the motors in the azimuth and elevation axes of the turret system during the simulation of scenario 3, with the fire target located 60 m away and 30 m above the robot.
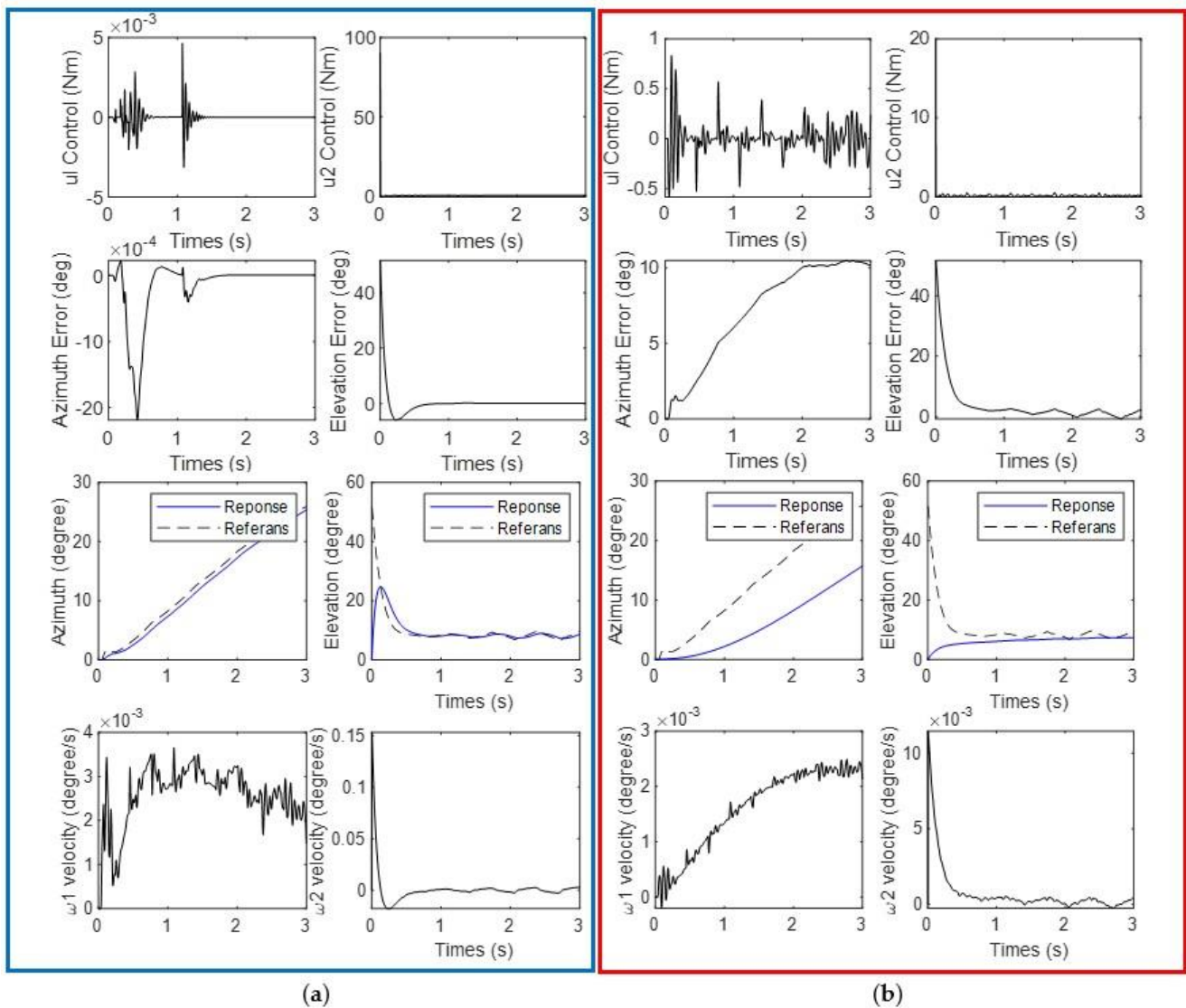
Figure 18. Control signals, error values, trajectory and velocity of Turret System elevation and azimuth motor with (**a**) SMC (**b**) PID controllers for Scenario 3.

4. Discussion

The firefighter robot fired at 35 fire target coordinates at a horizontal distance of 20–80 m and a vertical distance of 1–30 m for three different scenarios. In order to demonstrate and compare the turret stabilization success of SMC and PID controllers, the response performance metrics of the controllers are presented numerically in Table 9. The shots outside the 5 m circle are written in bold in the tables. It is seen that the performance of the SMC controller is better than the PID controller for all three scenarios. It is clear that turret stabilization will also have a linear effect on shooting accuracy.

Table 9. Response performance of PID and SMC controller for turret system.

Metrics	Turret Axes	Scenario 1		Scenario2		Scenario 3	
		PID	SMC	PID	SMC	PID	SMC
Max. steady-state tracking error (degree)	Azimuth	0.0002	0.0001	0.035	0.0167	10.42	1.179
	Elevation	1.78	0.172	1.4	0.193	2.53	0.019

In Table 10, the fire-extinguishing ball hit success rate obtained with the SMC and PID controllers applied to the turret system is shown.

Table 10. Shooting performance for all scenarios.

No	Target Distance and Height (m)	Total Distance (m)	The Percentage Firing Fault of Hit/Firing Accuracy Value Scenario 1		The Percentage Firing Fault of Hit/Firing Accuracy Value Scenario 2		The Percentage Firing Fault of Hit/Firing Accuracy Value Scenario 3	
	Controller Type		PID	SMC	PID	SMC	PID	SMC
1	20 m/1 m	20.024	3.645625	4.721334	2.497004	3.604175	2.147423	**8.682581**
2	20 m/5 m	20.615	4.123211	3.835072	3.298569	2.778074	3.056027	**8.032016**
3	20 m/10 m	22.360	4.516995	2.699463	4.025045	1.757156	4.069767	**7.021467**
4	20 m/20 m	28.284	**5.055862**	0.948239	4.914439	0.274714	**5.621553**	5.168647
5	20 m/30 m	36.055	**5.741229**	0.034947	**5.685758**	0.573291	6.989322	3.950631
6	30 m/1 m	30.016	1.965618	3.086687	0.59968	2.343417	0.333156	**5.759262**
7	30 m/5 m	30.413	2.630454	2.631769	1.44675	1.913655	1.315227	**5.462467**
8	30 m/10 m	31.622	3.257226	2.040352	2.276896	1.368351	2.40339	**5.02182**
9	30 m/20 m	36.055	3.910692	0.976286	3.217307	0.424906	4.049369	4.11316
10	30 m/30 m	42.426	4.006977	0.210484	3.370575	0.263518	**5.161929**	3.375996
11	40 m/1 m	40.012	0.749775	2.256573	0.69979	1.70124	1.049685	4.289463
12	40 m/5 m	40.311	1.488427	1.969934	0.099228	1.428642	0.793828	4.115006
13	40 m/10 m	41.231	2.255584	1.598554	0.994397	1.08171	1.527977	3.867721
14	40 m/20 m	44.721	3.13052	0.889739	2.034838	0.438944	3.13052	3.347197
15	40 m/30 m	50	2.8	0.309	1.62	0.114	4.2	2.883
16	50 m/1 m	50.009	0.199964	1.749285	1.359755	1.306965	1.71969	3.402987
17	50 m/5 m	50.249	0.995045	1.547294	0.537324	1.114251	1.213955	3.286235
18	50 m/10 m	50.990	1.804275	1.287311	0.333399	0.869582	1.431653	3.126888
19	50 m/20 m	53.851	2.636906	0.777887	1.207034	0.401478	2.766894	2.793449
20	50 m/30 m	58.309	1.492051	0.329623	0.1715	0.066542	3.995953	2.484522
21	60 m/1 m	60.008	0.316624	1.402646	1.34982	1.036029	1.749767	2.675977
22	60 m/5 m	60.207	1.096218	1.250021	0.5315	0.890096	1.361968	2.723936
23	60 m/10 m	60.827	1.857728	1.054466	0.197281	0.705279	1.627567	2.611998
24	60 m/20 m	63.245	2.150368	0.666614	0.4111	0.345798	2.830263	2.381532
25	60 m/30 m	67.082	0.954056	0.310515	3.041054	0.058883	**5.172774**	2.165857
26	70 m/1 m	70.007	0.971331	1.146742	0.771351	0.834631	1.442713	2.379762
27	70 m/5 m	70.178	1.595942	1.025535	0.185243	0.718601	1.496195	2.315968
28	70 m/10 m	70.710	1.99406	0.870881	0.155565	0.571913	1.99406	2.233065
29	70 m/20 m	72.801	0.618123	0.561805	1.387344	0.286535	3.57138	2.065356
30	70 m/30 m	76.157	**6.460339**	0.270625	**8.797615**	0.051341	**9.690508**	1.909214
31	80 m/1 m	80.006	1.562383	0.946554	0.299978	0.675574	1.59988	2.080469
32	80 m/5 m	80.156	1.646789	0.846474	0.274465	0.579744	2.021059	2.005464
33	80 m/10 m	80.622	1.004689	0.719159	1.004689	0.458808	2.790802	1.941778
34	80 m/20 m	82.462	4.28076	0.463971	**6.451456**	0.220465	**7.445854**	1.815624
35	80 m/30 m	85.440	**17.63811**	0.219101	**19.99064**	0.046582	**20.10768**	1.700023

➢ In the shooting simulation, the transformable wheeled robot struck 41 of the 105 targets with less than 1% error and 49 with a maximum error of 5% using the PID controller. Fifteen shots had an error rate greater than 5% and were judged unsuccessful.

➢ Using the SMC controller, the transformable wheeled robot hit 42 of the 105 targets with an error of less than 1% and 56 with a maximum error of 5% in its shooting simulation. Seven of its shots had an error rate of more than 5% and were deemed unsuccessful.

It can be shown that the SMC controller is more effective in dampening vibrations in the hull sent to the turret system. As the stabilization improved, the accuracy of the ball increased. SMC's hit success rate, especially at distant targets far away 50 m, is 15% better than PID.

5. Conclusions

A transformable six-wheeled firefighter robot was designed in this study. The fire extinguisher ball can be thrown using the robot's two-degrees-of-freedom shooting turret. In the context of this study, a three-dimensional simscape model was constructed in the Matlab Simmechanic environment after first creating a kinematic model of the turret system and the concept design for the robot. Control of the fire extinguisher is simulated against fixed targets with known coordinates using the turret mechanism on the firefighter robot. The turret was stabilized using PID and SMC controllers, and their results were compared. The success of the turret in firing has been shown in the first simulation, when the robot is in a stable location and there are no movement-related oscillations in the hull. The success of the controllers in keeping the turret barrel on target and the shooting accuracy performances of the controllers as the robot moves on the fingers at a steady speed are demonstrated in the second simulation. In the third simulation, while the firefighter robot rotates 90 degrees around itself, the targets were fired. It is seen that the turret system stabilization success of the SMC controller is much higher than the PID controller in three scenarios. This is because SMC has a more robust property against shifting disturbance effects. If the hit success of each controller for all three scenarios is compared, 90/105 (85.71%) of shots with the PID controller and 100/105 (95.23%) of shots with the SMC controller propelled the fire-extinguishing ball within the 5% target circle and were considered successful.

6. Future Works

Studies on this topic are still being conducted within the parameters of the project. Using a three-dimensional concept design, stabilization control, and firing performance in the Simscape multibody simulation environment, a firefighting robot with a shooting turret will be created in this article. The prototype to be produced will include camera and IMU sensor modules to detect environmental and surface type. The prototype for the three scenarios provided in this paper will be the subject of actual experimental studies.

Data Availability Statement: All data used to support the findings of this study are included in the article.

Conflicts of Interest: The author declares no conflict of interest.

References

1. Avci, M.; Korkmaz, M. Türkiye'de orman yangını sorunu: Güncel bazı konular üzerine değerlendirmeler. *Turk. J. For.* **2020**, *22*, 229–240. [CrossRef]
2. TOD, Success in Fighting Forest Fires, Gaining Public Trust and Ensuring Work and Life Safety of Personnel, Turkish Foresters Association (TOD) Press Release. 2020, pp. 1–8. Available online: https://www.ormancilardernegi.org/Documents/d3bb64d5-0f58-4449-81de-5e9dc1b9436c.pdf (accessed on 30 January 2023).
3. Bogue, R. The role of robots in firefighting. *Ind. Robot. Int. J. Robot. Res. Appl.* **2021**, *48*, 174–178. [CrossRef]
4. Campanharo, W.A.; Lopes, A.P.; Anderson, L.O.; da Silva, T.F.M.R.; Aragão, L.E.O.C. Translating fire impacts in Southwestern Amazonia into economic costs. *Remote Sens.* **2019**, *11*, 764. [CrossRef]
5. Kang, R.; Fu, G.; Yan, J. Analysis of the Case of Fire Fighters Casualties in the Building Collapse. *Procedia Eng.* **2016**, *135*, 343–348. [CrossRef]
6. Oliveira, L.F.P.; Moreira, A.P.; Silva, M.F. Advances in Forest Robotics: A State-of-the-Art Survey. *Robotics* **2021**, *10*, 53. [CrossRef]
7. Mass, C.F.; Ovens, D. The Northern California Wildfires of 8–9 October 2017: The Role of a Major Downslope Wind Event. *Bull. Am. Meteorol. Soc.* **2019**, *100*, 235–256. [CrossRef]
8. Wang, Y.; Xing, J.-P.; Guo, H.; Wang, L.-J. Key Technologies of Tunnel Firefighting Robots. *IETE Tech. Rev.* **2016**, *34*, 3–10. [CrossRef]
9. Tan, G.W.M.R.C.F.; Liew, S.M.; Alkahari, M.R.; Ranjit, S.S.S.; Said, M.R.; Chen, W. Fire Fighting Mobile Robot: State of the Art and Recent Development. *Aust. J. Basic Appl. Sci.* **2013**, *7*, 220–230.
10. Zhang, J.; Jin, Z.; Zhao, Y. Dynamics analysis of leg mechanism of six-legged firefighting robot. *J. Mech. Sci. Technol.* **2018**, *32*, 351–361. [CrossRef]

11. Guo, A.; Jiang, T.; Li, J.; Cui, Y.; Li, J.; Chen, Z. Design of a small wheel-foot hybrid firefighting robot for infrared visual fire recognition. *Mech. Based Des. Struct. Mach.* **2021**, 1–20. [CrossRef]

12. Li, S.; Feng, C.; Niu, Y.; Shi, L.; Wu, Z.; Song, H. A Fire Reconnaissance Robot Based on SLAM Position, Thermal Imaging Technologies, and AR Display. *Sensors* **2019**, *19*, 5036. [CrossRef]

13. Li, J.; Wang, J.; Peng, H.; Hu, Y.; Su, H. Fuzzy-Torque Approximation-Enhanced Sliding Mode Control for Lateral Stability of Mobile Robot. *IEEE Trans. Syst. Man, Cybern. Syst.* **2021**, *52*, 2491–2500. [CrossRef]

14. Aliff, M.; Samsiah, N.; Yusof, M.; Zainal, A. Development of Fire Fighting Robot (QRob). *Int. J. Adv. Comput. Sci. Appl.* **2019**, *10*, 142–147. [CrossRef]

15. Ando, H.; Ambe, Y.; Ishii, A.; Konyo, M.; Tadakuma, K.; Maruyama, S.; Tadokoro, S. Aerial Hose Type Robot by Water Jet for Fire Fighting. *IEEE Robot. Autom. Lett.* **2018**, *3*, 1128–1135. [CrossRef]

16. McNeil, J.G.; Lattimer, B.Y. Robotic Fire Suppression Through Autonomous Feedback Control. *Fire Technol.* **2016**, *53*, 1171–1199. [CrossRef]

17. Zhu, J.; Li, W.; Lin, D.; Cheng, H.; Zhao, G. Intelligent Fire Monitor for Fire Robot Based on Infrared Image Feedback Control. *Fire Technol.* **2020**, *56*, 2089–2109. [CrossRef]

18. Jiang, H. Mobile Fire Evacuation System for Large Public Buildings Based on Artificial Intelligence and IoT. *IEEE Access* **2019**, *7*, 64101–64109. [CrossRef]

19. Chen, Z.; Wang, S.; Wang, J.; Xu, K.; Lei, T.; Zhang, H.; Wang, X.; Liu, D.; Si, J. Control strategy of stable walking for a hexapod wheel-legged robot. *ISA Trans.* **2020**, *108*, 367–380. [CrossRef] [PubMed]

20. Kim, J.-H.; Starr, J.W.; Lattimer, B.Y. Firefighting Robot Stereo Infrared Vision and Radar Sensor Fusion for Imaging through Smoke. *Fire Technol.* **2014**, *51*, 823–845. [CrossRef]

21. Kim, J.-H.; Lattimer, B.Y. Real-time probabilistic classification of fire and smoke using thermal imagery for intelligent firefighting robot. *Fire Saf. J.* **2015**, *72*, 40–49. [CrossRef]

22. Kim, J.; Kim, B.K. Cornering Trajectory Planning Avoiding Slip for Differential-Wheeled Mobile Robots. *IEEE Trans. Ind. Electron.* **2019**, *67*, 6698–6708. [CrossRef]

23. Pransky, J. Geoff Howe, senior vice president, Howe and Howe, Inc., a subsidiary of Textron Systems; co-pioneer of robotic firefighting technologies, including Thermite™ firefighting robots. *Ind. Robot. Int. J. Robot. Res. Appl.* **2021**, *48*, 169–173. [CrossRef]

24. Statistics Sweden. Design Your Questions Right: How to Develop, Test, Evaluate and Improve Questionnaires 2004. Available online: http://www.scb.se/statistik/_publikationer/OV9999_2004A01_BR_X97OP0402.pdf. (accessed on 6 June 2020).

25. Magirus, Magirus AirCore. 2019. Available online: https://www.magirusgroup.com/de/en/products/special-vehicles/aircore/ orhttps://www.magirusgroup.com/de/de/produkte/spezialfahrzeuge/aircore/ (accessed on 6 May 2022).

26. Shark Robotics. Colossus. 2020. Available online: https://www.shark-robotics.com/shark-robots (accessed on 6 May 2022).

27. Milrem Robotics, Multiscope Rescue with Hydra. 2020. Available online: https://milremrobotics.com/product/multiscope-rescue-hydra/ (accessed on 6 May 2022).

28. Milrem Robotics, Multiscope Rescue Hose Cartridge. 2020. Available online: https://milremrobotics.com/product/firehouse-container/ (accessed on 6 May 2022).

29. Župančić, I. Special robotized multipurpose vehicle DOK-ING MVF-5. *Vatrog. I Upravlj. Požarima* **2012**, *2*, 17–35.

30. Apparatus, F. Firefighting Robotic Vehicle System. 2020. Available online: https://www.fireapparatusmagazine.com/fireapparatus/firefighting-robotic-vehicle-system/#gref (accessed on 6 May 2022).

31. LUF. LUF60 Fire Frighter. 2019, p. 1. Available online: https://www.luf60.at/wp-content/uploads/sites/62/2019/07/luf_60_en.pdf (accessed on 30 January 2023).

32. Ryland Research. Fire-Fighting Robotics. 2010. Available online: https://rylandresearch.com/research-and-development/fire-fighting-robotics/ (accessed on 30 January 2023).

33. Zhao, J.; Zhang, Z.; Liu, S.; Tao, Y.; Liu, Y. Design and Research of an Articulated Tracked Firefighting Robot. *Sensors* **2022**, *22*, 5086. [CrossRef] [PubMed]

34. Murph, D. ARMTEC' s SACI firefighting robot. 2006. Available online: https://www.engadget.com/2006-08-03-armtecs-saci-firefighting-robot.html (accessed on 30 January 2023).

35. Firefighting Robots. 2022. Available online: https://www.allonrobots.com/firefighting-robots/ (accessed on 30 January 2023).

36. MyBOT-X. The First Malaysia Fire Fighting Robot. 2013. Available online: https://www.robolab.com.my/wp-content/uploads/2019/05/MyBOT-X-series_007_2018.pdf (accessed on 30 January 2023).

37. VisitFinland, MHI Develops Autonomous 'Water Cannon Robot' and 'Hose Extension Robot' for Use in Firefighting—Expected to Play Active Role in Hazardous Situations Inaccessible to Firefighting Crews. 2019. Available online: https://www.mhi.com/news/190325.html (accessed on 30 January 2023).

38. Debbie Sniderman, Robotic Firefighting Vehicles. 2011. Available online: ASME.org (accessed on 30 January 2023).

39. Deliverable, S. Mobile Robots with Novel Environmental Sensors for Inspection of Disaster Sites with Low Visibility Software Toolkit. *Data Vis.* **2018**, *40*, 1–5.

40. Dobric, J. SmokeBot—A Robot Serving Rescue Units. 2018. Available online: https://www.oru.se/english/news/news-archive/news-archive-2018/smokebot--a-robot-serving-rescue-units/ (accessed on 30 January 2023).

41. Zhang, J.; Jin, Z.; Feng, H. Type synthesis of a 3-mixed-DOF protectable leg mechanism of a firefighting multi-legged robot based on GF set theory. *Mech. Mach. Theory* **2018**, *130*, 567–584. [CrossRef]

42. Tatar, A.B.; Tanyıldızı, A.K.; Yakut, O. Four-legged hunter (FLH) robot: Design and shooting control to moving targets with SMC. *Simul. Model. Pract. Theory* **2020**, *104*, 102117. [CrossRef]

43. Çakar, O.; Tanyıldızı, A.K. Application of moving sliding mode control for a DC motor driven four-bar mechanism. *Adv. Mech. Eng.* **2018**, *10*. [CrossRef]